Case Studies in Construction Materials 17 (2022) e01208

Contents lists available at ScienceDirect

Case Studies in Construction Materials

journal homepage: www.elsevier.com/locate/cscm

Short communication

Monitoring of chloride and Friedel's salt, hydration components, and porosity in high-performance concrete

Erniati Bachtiar [a,*], Fatmawaty Rachim [a], Ritnawati Makbul [b], Arbain Tata [c], Muhammad Irfan-Ul-Hassan [d], Mehmet Serkan Kırgız [e], Muhammad Syarif [f], André Gustavo de Sousa Galdino [g], Anwar Khitab [h], Omrane Benjeddou [i], Konstantinos G. Kolovos [j], Enrique Fernandez Ledesma [k], Andi Yusri [f], Styliani Papatzani [l]

[a] *Department of Civil Engineering, Fajar University, Makassar, South Sulawesi, Indonesia*
[b] *Department of Infrastructure and Environmental Engineering, Faculty of Engineering, Fajar University, Makassar, Indonesia*
[c] *Department of Civil Engineering, Universitas Khairun, Ternate, Indonesia*
[d] *Department of Civil Engineering, University of Engineering & Technology, Lahore, Pakistan*
[e] *Department of Architecture, Faculty of Engineering and Natural Sciences, İstanbul Sabahattin Zaim University, Küçükçekmece 34303, İstanbul, Turkey*
[f] *Department of Architecture, Univeristas Muhammadiyah Makassar, Indonesia*
[g] *Federal Institute of Education, Sciences and Technology of Espírito Santo, Av. Vitória, 1729, Jucutuquara, Vitória, ES 29040–780, Brazil*
[h] *Department of Civil Engineering, Mirpur University of Science and Technology (MUST), Mirpur 10250, AJK, Pakistan*
[i] *Prince Sattam bin Abdulaziz University, College of Engineering, Department of Civil Engineering, Alkharj 16273, Saudi Arabia*
[j] *Hellenic Millitary Academy, Laboratory of Inorganic Chemistry, Vari, ATTICA, Greece*
[k] *Área de Ingeniería de la Construcción, EPS de BELMEZ, Universidad de Córdoba, Córdoba, Spain*
[l] *Department of Surveying and Geoinformatics Engineering, School of Engineering, University of West Attica, 250 P. Ralli & Thivon, 122 44 Egaleo, Greece*

ARTICLE INFO

Keywords:
High-performance concrete
Curing of seawater and air
Seawater as mixing component
Analyzis of XRD, Petrography, and SEM
Porosity
Chloride and Friedel's salt

ABSTRACT

The innovative paper evaluated the water of the sea as a curing component and mixing constituent in high-performance concrete (HPC). This motivation would provide an understanding for the reader of how the water from the sea affects the HPC. This paper would provide information about the mechanism and the influence of prepared high-performance concrete mixed with either freshwater or seawater and made to cure in freshwater, seawater, or air. The mechanism and the influence were evaluated by XRD tests, SEM observations, and petrography analysis of HPCs at 3 days, 7 days, 28 days, and 90 days. The structure of the Friedel's salt increases tobermorite and ettringite ($3CaO.Al_2O_3.3CaSO_432H_2O$) and retards portlandite ($Ca(OH)_2$) and calcium silicates ($2CaO.SiO_2$ and $3CaO.SiO_2$) in HPC mixed with seawater for 3–90 days. Air curing reduces the formation of portlandite ($Ca(OH)_2$), tobermorite ($3CaO.2SiO_2.3H_2O$), ettringite ($3CaO.Al_2O_3.3CaSO_432H_2O$), and calcium silicate ($3CaO.SiO_2$) in seawater HPC while increasing the formation of calcium silicate ($2CaO.SiO_2$). SEM analysis supports the mechanism and influence of mixing of seawater, curing in the water of the sea, and curing treatment in the air. According to data from petrographic analysis and porosity testing, the porosity was decreased by the seawater and curing treatment in the seawater in HPC mixes. In terms of hydration

* Corresponding author.
E-mail address: erni_nurzaman@yahoo.com (E. Bachtiar).

https://doi.org/10.1016/j.cscm.2022.e01208
Received 20 March 2022; Received in revised form 20 May 2022; Accepted 30 May 2022
Available online 9 June 2022

components, SEM observation, porosity, and petrographic analysis, the HPC-3 shows the best performance in the work.

1. Introduction

Currently curing of concrete in freshwater is the most widely-used method for concrete constructions and structural materials worldwide because of its easy-to-use. Nevertheless, it is estimated that there may be a shortage of mainstream of freshwater in terms of population increase and misusing of freshwater resources [1,2]. The use of saltwater in place of freshwater for curing and mixing of concrete might be an efficient technique to save freshwater resources. Due to the high salt content of saltwater and its corrosive impact on construction steel, its use in reinforced concrete was prohibited [3]. Nevertheless, high-strength concrete (HSC) and fiber-reinforced composite (FRC) could make the using of seawater become an actuality in both curing and mixing purposes for sustainability and durability of concrete [4–6]. On the other hand, since the surface of the earth has an extensive sea area and the sea contains abundant water that is to meet human needs in the world, the settlement in front of sea is important. This need can be enumerated in food sources (fish and marine plants), energy sources (petroleum and wave power plants), transportation, and tourist attractions. Therefore, humans would like to take advantage of the settlement in front of the sea as much as possible. To utilize the various advantages, various supporting infrastructure was built on the sea coast or above the sea. The supporting infrastructure built is seaports, offshore platforms, bridges, and resting places (rest area), etc [7]. Additionally, marine environment is an area with aggressive chemicals, e.g., salt and chlorine. The degradation of reinforced concrete structures (RCS) exposed aggressive chemicals in marine circle could happen because of attack of chloride ion and saturation of carbon di oxide [8]. The reinforced concrete structure encounters the attack of chloride ions because of deicing seawater, salt, and simultaneously the greenhouse-gas releasing [9,10]. The movement of chloride ions via the microcracks and porosity structure of concrete may result in decreased the durability of reinforced concrete structure, as well as the dissolution of the oxide on construction steel which is coated by the cement matrix, hence accelerating corrosion. [11–13]. The chlorine ions are absorbed by the cement-based matrix as the salt of Friedel transports and develops [14,15]. Furthermore, chloride transport may be slowed by a process known as binding of chlorine, which is one of the most crucial steps of diffusion ion of chlorine. [16–19]. The stages of ionic binding may be divided into two categories: alchemy and physique [20]. The physique step occurs when cement hydration products, particularly gel of calcium-silica-hydrate, absorb chloride ions. The forming of salt of Friedel is regarded as the alchemy step [21,22]. On the one hand, this binding step slows the formation of free chloride in the pore solution, which reduces ion diffusion of chloride and delays ion reaching of chlorine in the construction steel. It also minimizes voids associated with the development of salt of Friedel, that prevents the distributing of other harmful minerals [14, 18].

On the other hand, construction of infrastructure in an aggressive environment such as the surrounding area or at sea needs to pay attention to the material used [7,23–25]. Buildings in an aggressive environmental area must be designed by considering the impact of an aggressive environment on the structure and materials. The sea area is an aggressive environment that can affect the materials used, especially concrete and steel buildings. Infrastructure construction is generally made of concrete and steel. The concrete used must be of high quality if used in an aggressive environment. As we know, the two materials, if contaminated with seawater, will affect the quality of the structural material. The corrosion of concrete and steel is influenced by saltwater containing salt solutions, particularly alkali (NaCl) and heptahydrate ($MgSO_4$). [26,27]. Due to the increased quantity of ettrengite production caused by the presence of sulfate salts, the hardened concrete matrix is harmed, leading to a large increase in volume in the hardened concrete matrix. The large volume in the matrix provides internal stresses that cause cracks in the concrete mass to affect the resistance of concrete [26]. Concrete materials used in the construction of buildings in aggressive areas, in this case at sea, need high-quality concrete. High-strength concrete has high strength and low porosity. High-strength concrete can inhibit or minimize the entry of seawater to get to the concrete reinforcement. Besides that, high-strength concrete has high durability to avoid or minimize the corrosion process of concrete and reinforcement. Previous research on advance concrete, namely ultra-high-performance cement-based material made using water of sea and sand of sea, shown strength of compression as 180 MPa [27]. With increasing age, there will be a reduced in endurance and increased in porosity and absorption in the construction material [28]. Another current research on high-strength concrete that used seawater as mixing and treatment water showed greater initial strength than the concrete that used freshwater as mixing water [29, 30]. In addition, research on mortar and concrete using seawater showed that the endurance of grout and other cement-based material increased when applying water of sea as mixing constituent [31]. The development of high-performance-concrete employing saltwater and sand of sea as mixing and curing component resulted in a modest decrease in workability, elastic moduli, and bulk density. Additionally, it demonstrated a modest rise in the initial endurance immediately [32].

Considering explanation above, this paper provides a couple of benefits for construction that uses high-performance concrete (HPC) material in marine environment. However, making concrete cannot avoid seawater contamination; therefore, it would affect the concrete to undergo hydration process until it hardens. This paper describes the mechanism and influence of seawater mixing, seawater curing, and air curing in the HPC, with XRD quantitative analyzis of hydration component of HPC, SEM microstructural analyzis of HPC, porosity testing, and petrographic analyzis of HPC. The analyzises were carried out at the age from 3 days to 90 days.

Table 1
Composition of high performance concrete ingredients for one cubic meter and curing conditions.

Types of Concrete	Ingredients of mixture (kg/m^3)						Curing Conditions		
	Fresh water	Sea water	Cement	Sand	Gravel	SP	Water of fresh	Water of sea	Dry air
HPC-1	204	0	601.3	770.1	785.1	6	+	–	–
HPC-2	204	0	601.3	770.1	785.1	6	–	+	–
HPC-3	0	204	601.3	770.1	785.1	6	–	+	–
HPC-4	0	204	601.3	770.1	785.1	6	–	–	+

2. Preparation of material and its tests

2.1. Mixing constituent of HPC

The high performance concrete (HPC) utilized materials, namely freshwater, aggregate (crushed stone and sand), binder (Portland composite cement), and superplasticizer.

2.2. Methods

This study was divided into many stages: material preparation, mixture design, specimen manufacture, curing, and microstructural properties test. In addition, this work also used seawater, instead of fresh water in the mixing and in the curing, in case the concrete structure were made in an aggressive environment, like sea. For that aim, concretes were stored in a bath of sea water, measuring 2 m $\times$ 1.5 m $\times$ 0.5 m.

High-performance concrete with a compressive strength more than 50 MPa was used in this study. In the planning and production of concrete samples utilizing the self-compacting concrete process. For the mix-design of HPC, it was followed the method of the European Guideline of self-compacting concrete [33]. The water/cement was kept constant at 1.1 in the HPC mix design, as recommended by the EFNARC. The water/cement factor of 0.35 was determined in the formulation of the HPC mixture. The average slump flow value is 722.5 mm for HPC using fresh water as the mixed water and 678.5 mm for HPC using seawater as the mixing water. The slump flow value meets the workability requirements of concrete using the SCC method, which is between the values of 650–800 mm. The components and curing conditions for one cubic meter of high performance concrete are listed in Table 1.

A mixer is used in the process of mixing concrete. After all the mixture compositions remained homogeneous, the mixture was poured into a cylindrical mold with a size of 10 cm $\times$ 20 cm. After the concrete is dry, the sample is taken from the mold and placed in the air and immersed in seawater or fresh water to cure. Concrete samples are preserved for 3, 7, 28, and 90 days in air, seawater, or fresh water in an immersion bath. Concrete samples are preserved for 3, 7, 28, and 90 days in air, seawater, or fresh water in an immersion bath. After treatment and reaching the appropriate age, the samples were then tested for XRD, SEM, and petrography. Samples for testing and microstructural analysis (SEM, XRD, and petrography) were made by cutting cylindrical samples to sizes according to their respective test standards. The samples analyzed were between 0.5 and 2.0 cm from the cylindrical surface. The number of samples for each variation of concrete and the age variation of each sample for each measurement of SEM, XRD, and petrography is 1 sample.

2.3. Quantitative analysis with XRD and SEM for component of cloride and salt of Friedel and hydration components, and observation of porosity and petrography in HPC

The XRD test analyzed the quantity of the microstructural components in the HPC, namely tobermorite, portlandite, ettringite, salt of Friedel, alite, belite, aluminate, and ferrite. The quantitative analysis with XRD was conducted to the rules based on ASTM C1365–18 standard [34]. The high-performance-concrete microstructures were analyzed using SEM analysis using a Tescan Vega. The porosity of high-performance-concrete was measured and computed according to the ASTM C642–13 standard [35]. The petrographic test was used for petrographic test is used to determine the morphology, type, size, and number of pores in the high-performance-concrete. An Olympus BX 51-P polarizing microscope was utilized for the petrography test, which followed ASTM C856/C856M-20 guideline [36].

3. Findings and arguments

3.1. Analysis X-ray diffraction and quantitative hydration components of HPC for cloride and salt of Friedel

The results of the hydration components of HPCs are shown in Table 2, including the chloride content and Friedel's salt for each type of HPC. Table 2 shows the effects of the curing phases of fresh water, seawater, and air. In addition, it is also seen how the effect of curing time on each type of HPC. These four mixtures are concrete mixtures made of portland cement and aggregate and superplasticizer and fresh water or sea water, which are preserved either in fresh water or sea water or air. The data shows that all of the hardened specimens have major clinker phases such as portlandite, tobermorite, ettringite, tri-calcium silicate, and di-calcium silicate, which are very similar to each other. Type HPC-1 proves that there is no chloride or Friedel's salt content. HPC-2 also showed that there

Table 2
Quantitative hydration component results of HPCs made of two different mixing water- fresh water and seawater and cured in three different conditions- freshwater, seawater, and air at 3, 7, 28 and 90 days.

Hydration components	Types of HPC															
	HPC-1				HPC-2				HPC-3				HPC-4			
	3	7	28	90	3	7	28	90	3	7	28	90	3	7	28	90
Portlandite ($Ca(OH)_2$) (%)	13.69	16.61	19.71	22.92	13.74	16.93	19.57	20.57	12.63	13.9	15.08	15.7	13.49	14.52	17.7	18.16
Tobermorite ($3CaO.2SiO_20.3\ H_2O$) (%)	26.32	34.27	39.42	45.83	25.31	38.09	42.5	45.94	31.58	36.36	43.24	46.74	30.71	33	39.27	42.29
Salt of Friedel ($3CaO.Al_2O_3.CaCl_2.10H_2O$)(%)	–	–	–	–	–	1.59	5	6.4	0.42	1.07	5.54	6.86	0.15	0.22	0.36	0.37
Ettringite ($3CaO.Al_2O_3.\ CaSO_4.32\ H_2O$) (%)	1.05	1.35	3.53	6.25	1.34	2.12	3.26	7.66	1.05	2.14	5.32	7.09	0.06	0.11	0.24	0.25
Chloride (Cl_2) (%)	–	–	–	–	–	1.06	2.17	3.77	4.84	5.35	5.54	5.93	2.06	2.53	1.45	1.62
Tricalcium silicate ($3CaO.SiO_2$) (%)	25.26	15.58	10.37	8.33	23.97	13.76	7.93	5.37	21.05	13.37	9.76	6.98	22.41	17.71	13.1	12.44
Dicalcium silicate ($2CaO.SiO_2$) (%)	33.68	32.19	26.97	16.67	35.64	26.45	19.57	10.29	28.43	27.81	15.52	10.70	31.12	31.91	27.88	24.87
Tetra-calcium Aluminoferrit (%)	–	–	–	–	–	–	–	–	–	–	–	–	–	–	–	–
Tri-calcium aluminate (%)	–	–	–	–	–	–	–	–	–	–	–	–	–	–	–	–
Total (%)	100	100	100	100	100	100	100	100	100	100	100	100	100	100	100	100

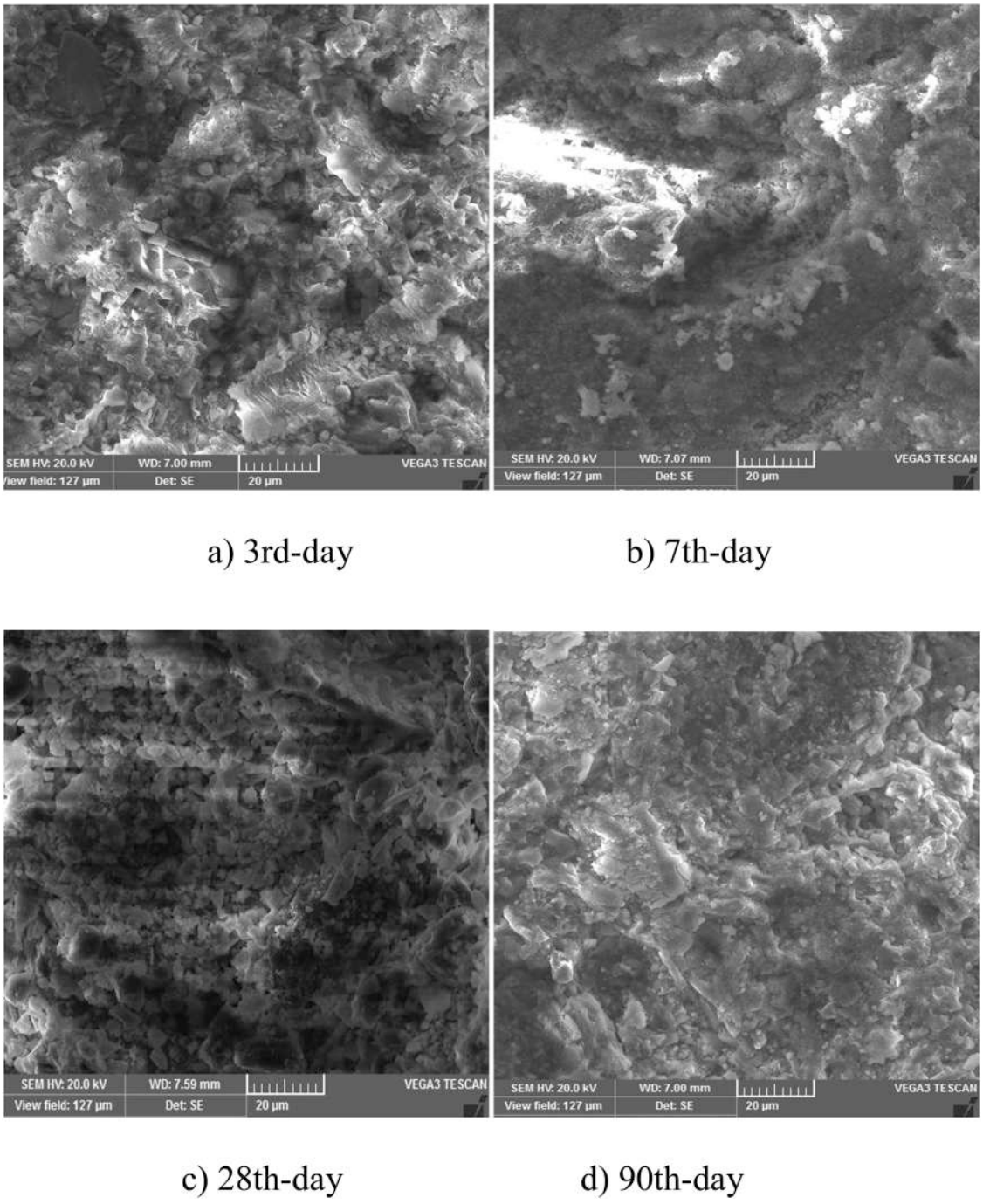

Fig. 1. SEM microstructure of HPC-1 made of water of fresh and cured into water of fresh for analyzing the influence of chloride content and salt of Friedel on micro-structure in HPC-1 at various curing ages.

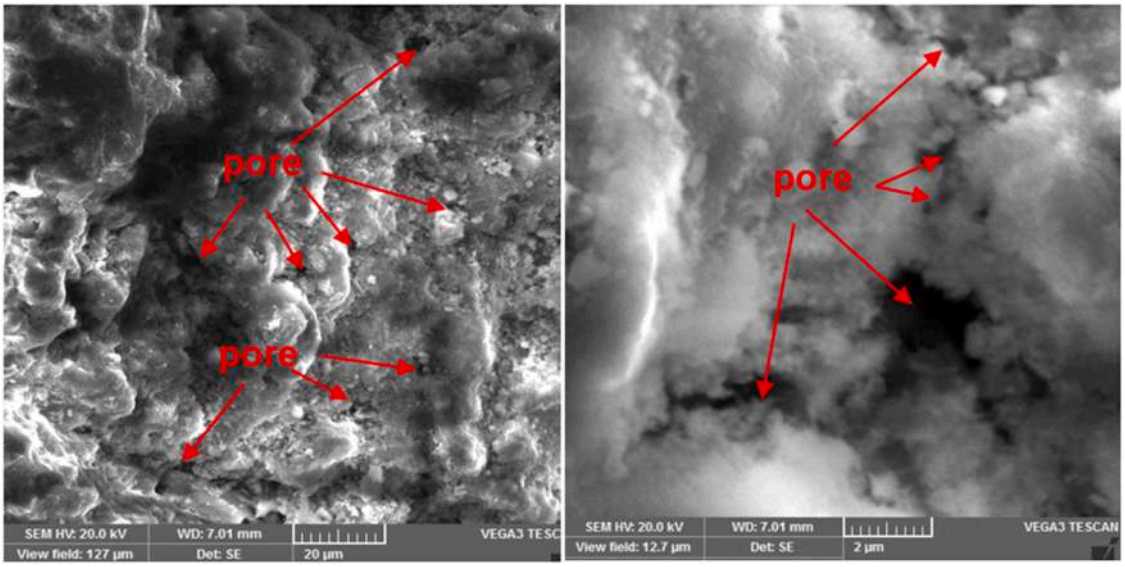

Fig. 2. SEM microstructure of HPC-1 made of water of fresh and treated in curing of water of fresh for 1 day to examine morphology and its impact on both hydration components and chloride and salt of Friedel levels in HPC-1.

was no chloride and no Friedel salt content at 3 days, even though it was preserved in seawater. However, starting at the age of 7 days, the curing effect of seawater has entered the concrete. Both HPC-3 and HPC-4 derive their chloride content and Friedel's salt component because they are both seawater and preserved in both seawater and air. Also, the HSC-4 sample showed that even though it wasn't kept in seawater, it still had chloride content and Friedel's salt because it had been mixed with seawater.

During immersion in HPC seawater, HPC-3 showed the highest chloride and friedel salt content. With increasing chloride content and Friedel's salt, the tobermorite component, which is the main strength contributing component, increases in HPC-3. The same increasing trend in tobermorite was observed in HPC-4, as it was mixed with seawater. Tobermorite and tricalcium silicate were reduced in HPC-2 preserved in seawater, while portlandite, ettringite, and dicalcium silicate were increased. Furthermore, neither the chloride component nor Friedel's salt are formed.

HPC-1 shows the general hydration components of portland cement (Table 1). By comparing the results of the chloride content and Friedel's salt together with the hydration component, it is evident that seawater has different effects on the hydration characteristics of HPC. The air curing effect is lower than the sea water curing for HPC. The results are in line with what Dias and Papadakis [37,38] found in their study.

3.2. SEM analysis for microstructure of HPCs and mechanism of cloride content and Friedel's salt

SEM pictures reveal the chloride concentration, salt of Friedel, and their impact on hydration components in HPC at 3th-day, 7th-day, 28th-day, and 90th-day. Besides, Fig. 6 shows image of SEM microstructure of HPC-1 to analyse morphology in the HPC-1. As noted in the 3.1 section, differences were observed in the micro-structure among different concrete mixes in water of sea curing, which may have led to change in micro-structure of cement matrix, including chloride concentration, salt of Friedel, and calcium-silica-hydrate gel.

By comparing the results, there is primarily displaying the effect of curing of sea water, curing of air, and mixing of concrete with sea water in the SEM pictures of H-P-C-1, H-P-C-2, H-P-C-3, and H-P-C-4 at three, seven, twenty-eight, and ninety-day ages. The method by which concrete mixes with sea water and cures in sea water and air seems to be different for various HPCs. Due to the complete mixing and curing of HPC in sea water, the chloride content and Friedel's salt may expedite cement hydration, resulting in the creation of extra hydrates, as Li et al. [39], led to much solid gel in HPCs. While the average bond capacity of the binder gel in H-P-C-2, H-P-C-3, and H-P-C-4 was typically the same as in HPC-1, the chloride concentration and salt of Friedel may have contributed to the gels' stability (Fig. 1). The four images appear to have different microstructural situations. At 3th-day, outer surface of HPC-1 seems to be less uniform, less dense, and with a variety of pore diameters (Fig. 10a). As shown in Fig. 10b, HPC-1 at 7 days old has much uniform and dense surface than HPC-1 at 3 days old, and the void stance has reduced in comparison to HPC-1 at 3th-day. As seen in Fig. 1c, the surface of HPC-1 after 28 days is more homogenous and denser than that of HPC-1 at 3th-day and 7th-day, and the void situation is reduced in comparison to HPC-1 at 3th-day and 7th-day. As seen in Fig. 1d, outer surface of HPC-1 at 90 days is the most homogenous and dense in the microstructures of HPC-1, and the pore size is less than that of HPC-1 at 3th-day, 7th-day, and 28th-day. Therefore, when the age of HPC-1 mixed in water of fresh and cured in water of fresh increases, the microstructure becomes much

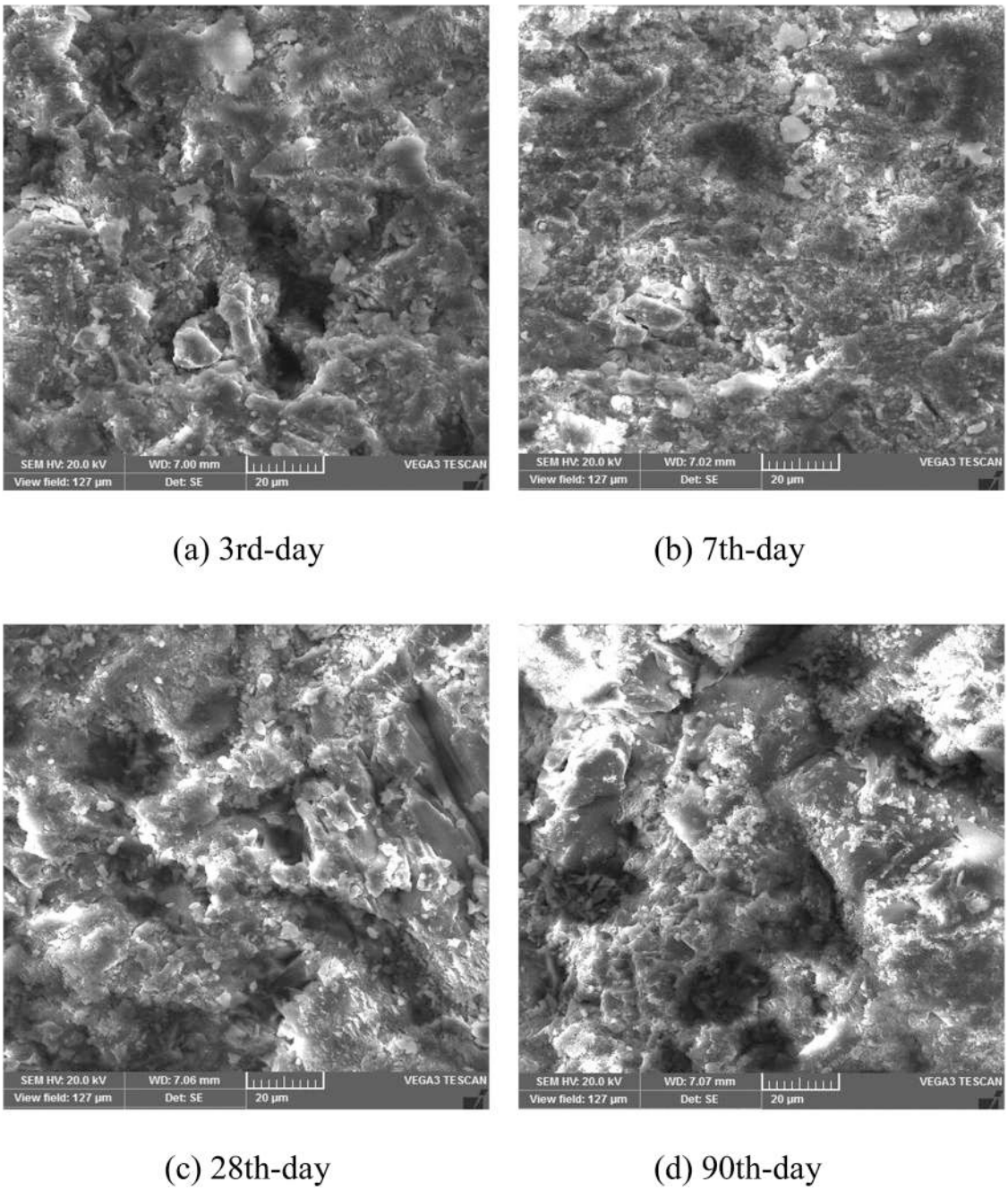

Fig. 3. SEM microstructure of HPC-2 mixed with water of fresh and cured in water of sea to analyse the influence of chloride content and salt of Friedel on microstructure in HPC-2 at various curing ages.

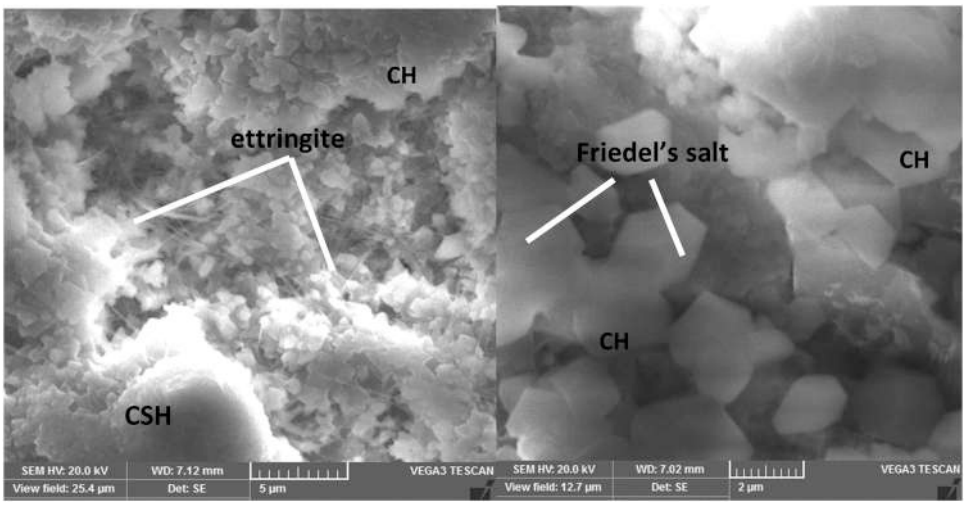

Fig. 4. Morphology of HPC-2 Microstructure using SEM, submerged in seawater for 28 days.

uniform and dense, and the pore volume decreases (Fig. 1).

The SEM image of microstructure of the HSC-1 mixed freshwater and cured in freshwater at 1 day old shows the formation of calcium-silica-hydrate gel (C-S-H), calcium hydroxide mass, and ettringite compounds. The calcium-silica-hydrate looks like a white flower shaped and the CH seems square mass and ettringite is a thin prism shaped needle (Fig. 3). The changes in hydration components could be attributed to the curing of seawater and mixing of concrete with water of sea. The corporation of water of sea curing and mixing of concrete with water of sea could optimize void and the compositions of hydration component and microstructure of C-S-H (Fig. 1 and 2). Fig. 3 displays SEM pictures of HPC-2 at 3th-day, 7th-day, 28th-day, and 90th-day to examine chloride concentration and salt of Friedel on HPC-2 microstructure. Besides, Fig. 4 displays the SEM microstructure of HPC-2 at 28 days to analyse morphology in the HPC-2.

The production of chloride content and salt of Friedel in HPC is a complex stage that is influenced by a variety of circumstances e.g., seawater curing, concrete mixing with water of sea, and exposure to a detrimental marine environment. This complicated process could be simplified by the work with SEM observation. It is obvious that once chloride content is not in the HPC-2 system, there is not Friedel's salt in HPC-2 system (Fig. 3). In other words, the salt of Friedel content grows as the chloride concentration increases. Friedel's salt would be more than 1.5% in the present HPC-2 system if the chloride concentration reaches 1%. Therefore, with the forming of chloride content, tobermorite increases and hydracalumite eventually converts into salt of Friedel, becoming the one-of-a-kind Friedel's salt. When chloride and salt of Friedel are added to the HPC-2 system, the chloride binding effect rises in solution. When the chloride concentration is sufficiently high, as it is in HPC-2 after 90 days, this process results in the forming of pure salt of Friedel and a rise in tobermorite in the HPC-2 system. The four photos seem to exhibit a variety of microstructural characteristics. At 3th-day, the presence of salt crystals was not readily apparent. The white salt crystals got clearer after 7th-day, 28th-day, and 90th-day. For further information, see Fig. 4, which depicts the crystal shape generated on HPC-2.

In the HPC-2 system, salt formation of Friedel exhibits unique properties. When the system's subatomic particles are limited to clor and hydroxide, no solid liquid is created. This is also supported by the shift in CH mass amount seen in Fig. 8. There is, however, an inverse effect. As a result, it may be deduced that the variable chloride content is due to salt of Friedel polymorphism (Figs. 3 and 4). Fig. 5 illustrates SEM examination of HPC3 at three-day, seven-day, 28-day, and 90-day ages to determine the chloride content and Friedel's salt concentrations, as well as their effect on hydration components in high-performance concrete. Additionally, Fig. 9 depicts the SEM microstructure of HPC-3 at 28 days for the purpose of analyzing HPC-3 morphology.

As can be observed from the SEM pictures, there is a clear distinction between HPC-3 and other HPCs after curing in either water of sea, water of fresh, or air. With turning out the chloride and Friedel's salt in HPC-3, the increase in the tobermorite led compact, dense, and bright microstructure to HPC-3 at 3 days (Fig. 5). Since the chloride content and Friedel's salt is very small and intermingling in SEM image of HPC-3 at 3 days, there is no visible in there. With next ages of HPC-3, there starts to be visible the chloride content and Friedel's salt (Fig. 6).

The hydration products are more numerous, the slurry gets thicker, and visible holes progressively reduce in HPC-3 over a period of three to ninety days. Numerous calcium hydroxide masses could be seen from the HPC-3, as well as a fibrous gel of calcium-silica-hydrate and a brilliant ettringite prism. Other components, such as aluminate, iron, and magnesium hydrates, and so on, are embedded in both the CH mass and the gel of calcium-silica-hydrate. After 90 days of saltwater curing, the tobermorite hydrate, CH mass, and C-S-H gel completely cover the microstructure of HPC-3. Literature also found that in Portland cement-based material containing sea water, at 63rd-day, the hydration rate could be slowed by unhydrated cement particle stack and water of sea [39]. Furthermore, the surface shape of hydration products between HPC-3 and HPC-1 is significantly different each other. A large number of prisims ettringite and masses CH and gel of calcium-silica-hydrate along with chloride content and salt of Friedel are found in HPC-3,

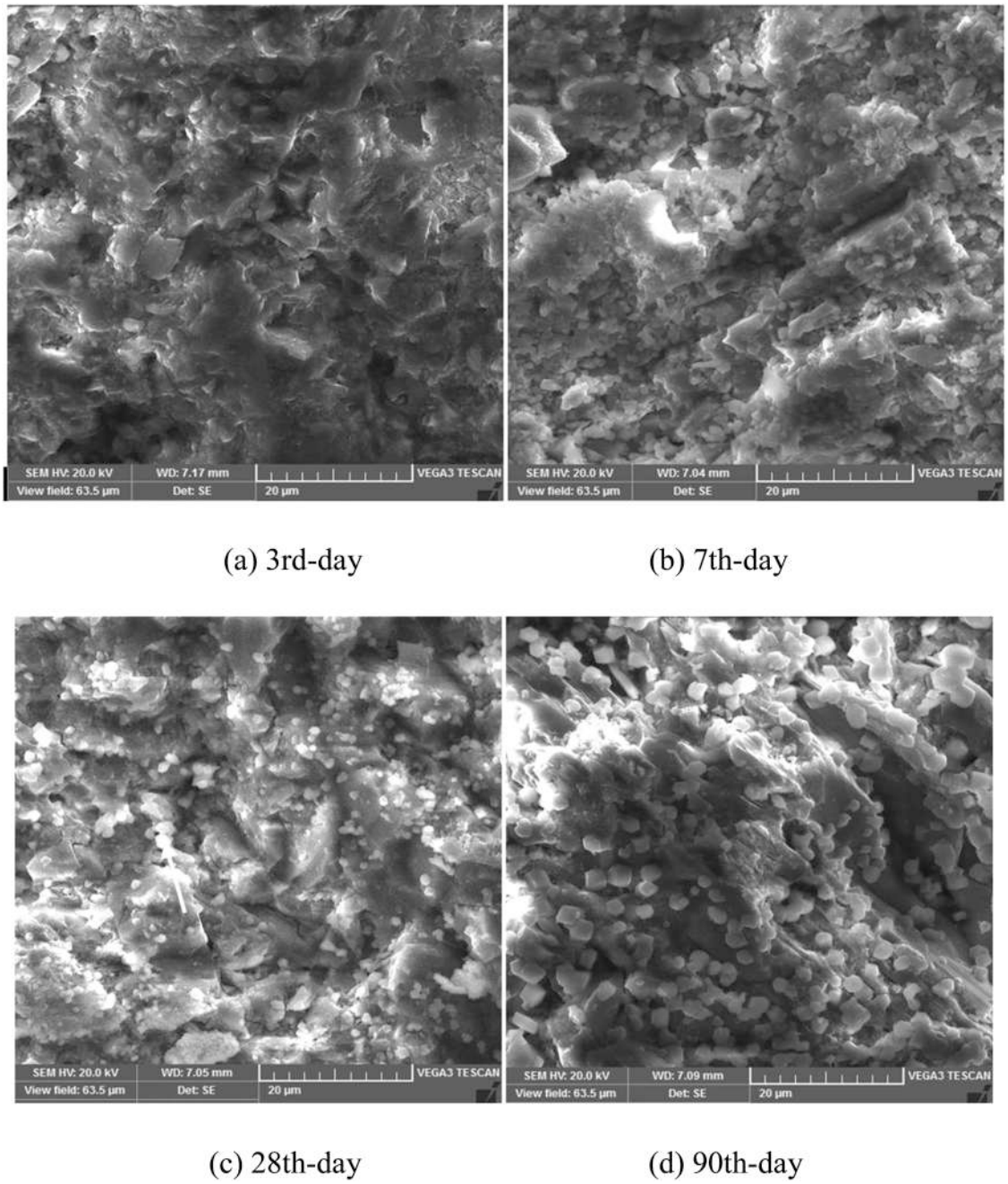

Fig. 5. SEM microstructure of HPC-3 with seawater curing.

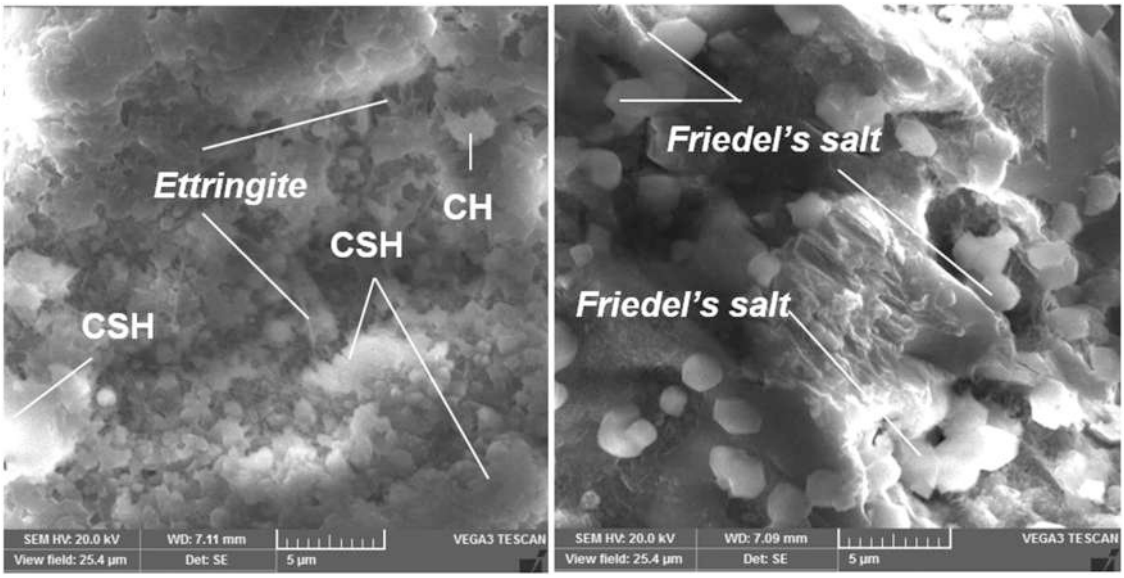

Fig. 6. SEM morphology of HPC-3 microstructure.

which are the hydration products of gypsum and tobermorite and oxide of silicate. As for the HPC-3, a large number of hydration products e.g., aluminates, ferrites, sulfates, peri-classes, and alkalis are strictly interlaced with CH mass and gel of calcium-silica-hydrate, making the microstructure of HPC-3 denser than that of other HPCs, therewith abbreviating the void of the HPC-3, which is dependable with the following petrography analysis. Fig. 4 displays pictures of SEM examination of HPC-4 at three different ages: three days, seven days, 28 days, and ninety days to examine the chloride content and salt of Friedel, as well as their impact on hydration components in high-performance concrete.

Fig. 7 displays pictures of SEM examination of HPC4 at three different ages: three days, seven days, 28 days, and ninety days to examine the chloride content and Friedel's salt, as well as their impact on hydration components in high-performance concrete. Besides, Fig. 8 shows image of SEM microstructure of HPC-4 at 90 days to analyse morphology in the HPC-4.

The hydration products of HPC-4 have been discovered through the research. It comprises salt of Friedel, chloride content, and carbonates in its micro-hydration-structure, in addition to gel of calcium-silica-hydrate, mass of calcium hydroxide, and ettringite. The chloride content led abundant Friedel's salt in HPCs as well as HPC-4. Younis et al. found that these corrosive expansive solutions result in the slight decrease in the porosity of HPCs [40]. Compared the HPC-4 with other HPCs in the work, there has a higher tobermorite, dicalcium silicate, and tricalcium silicate in the matrix. This also further shows that corrosive chloride content can accelerate the hydration of CH, gel of calcium-silica-hydrate, and ettringite to form a solid microstructure. Work published previously was shown that this acceleration can abbreviate the microstructure of HPCs [41]. Furthermore, with the rise in chloride component, there is hexagonal-shaped Friedel's salt the microstructure of HPC-4 at 90 days (Fig. 8). In HPCs, the calcium carbonate hydrated gradually increases because of air curing. It also demonstrates that, while air curing aids in the hydration of HPCs, HPC-4's matrix is denser than that of other HPCs. This outcome complies with literatüre's findings [40,41]. When comparing Fig. 8 to other figures of SEM images of HPCs, it can be seen that the micro-morphology of the interior mud of HPC-4 is identical after air curing. SEM and XRD analyses revealed that the hydration product chloride concentration in HSCs is comparable to the hydration products of salt of Friedel. This confirms that the effects of chloride and salt of Friedel on the micro-morphology of HPCs are identical.

3.3. Porosity and petrography analyzis of HPC

Regularly, there is an ongoing discussion regarding on the porosity of concrete. The shape and dissemination of void in HPC was not evaluated detailedly. The pore can be broadly classified into two groups to formation method and size: the entrained pore which is the smallest space with typical size of 0.1 μm and entrapped pore which is the largest space with typical size of greater than 1 μm. Void size is assumed to be evenly disseminated in this study, and Wang et al. also imply the same pattern [42,43]. There are air space, capillary void, gel void, and pore in cement-based materials. They are all different sizes, arranged, and linked [44]. The point regarding on void is that the durability of cement-based product is mainly affected by characteristic of porosity[45,46]. As one may expect, a smaller void in concrete combined with sufficient binding capacity results in increased concrete durability [47–50]. Mindess et al. has participated in the discussion on porosity. According to Mindess, the traditional categorization of void in concrete included two types: void of gel (<10 μm), that is connected with the creation of hydration product, and void of capillary (10 μm~10 000 μm), that are responsible for the majority of transport activities [51]. Additionally, the pore structure of cemant-based material contributes to diffusivity, e.g., chloride intrusion and Friedel's salt, which is mostly ascribed to the action of void of capillary and their connectedness [52]. Table 3

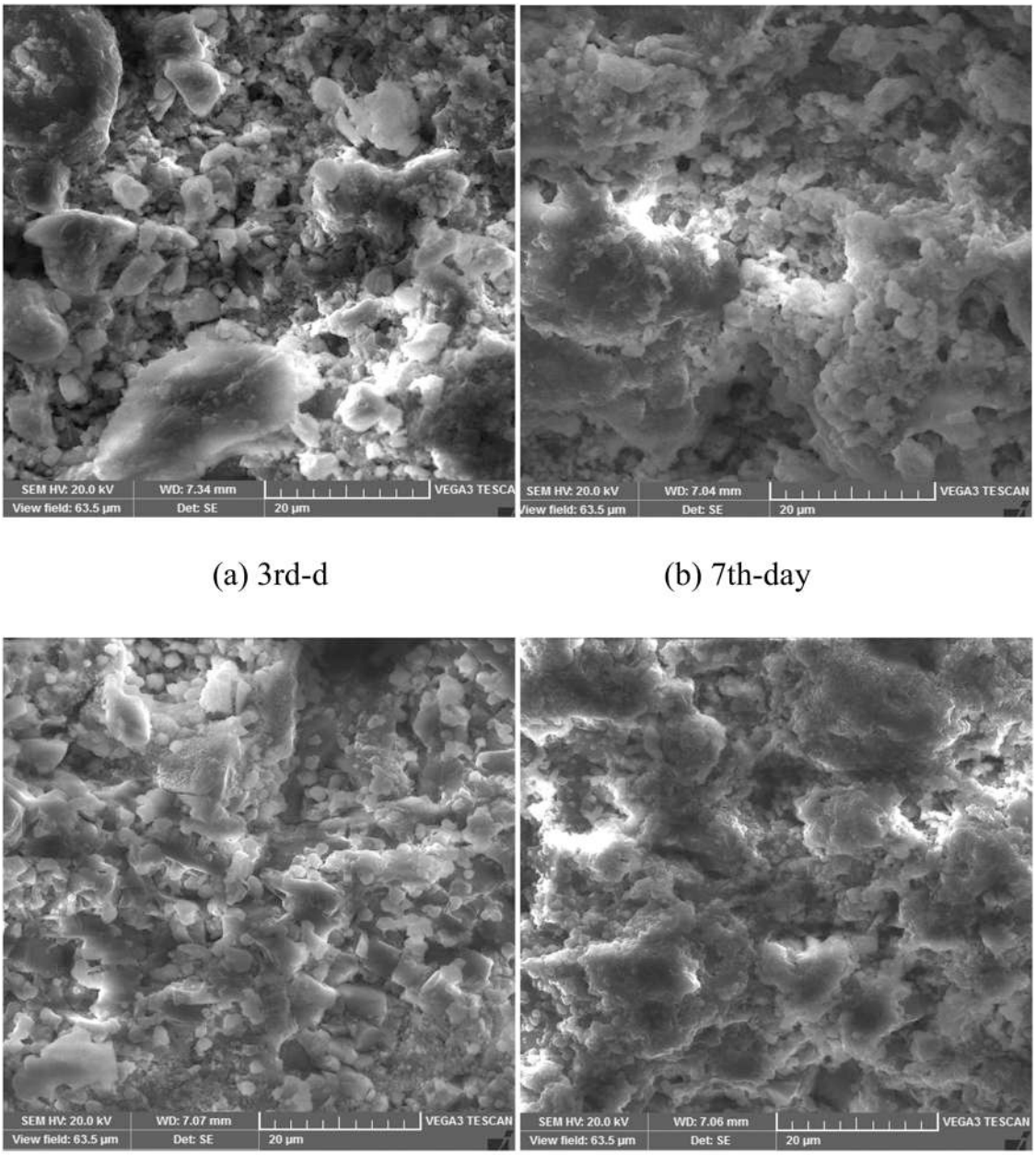

Fig. 7. SEM morphology of HPC-4 microstructure.

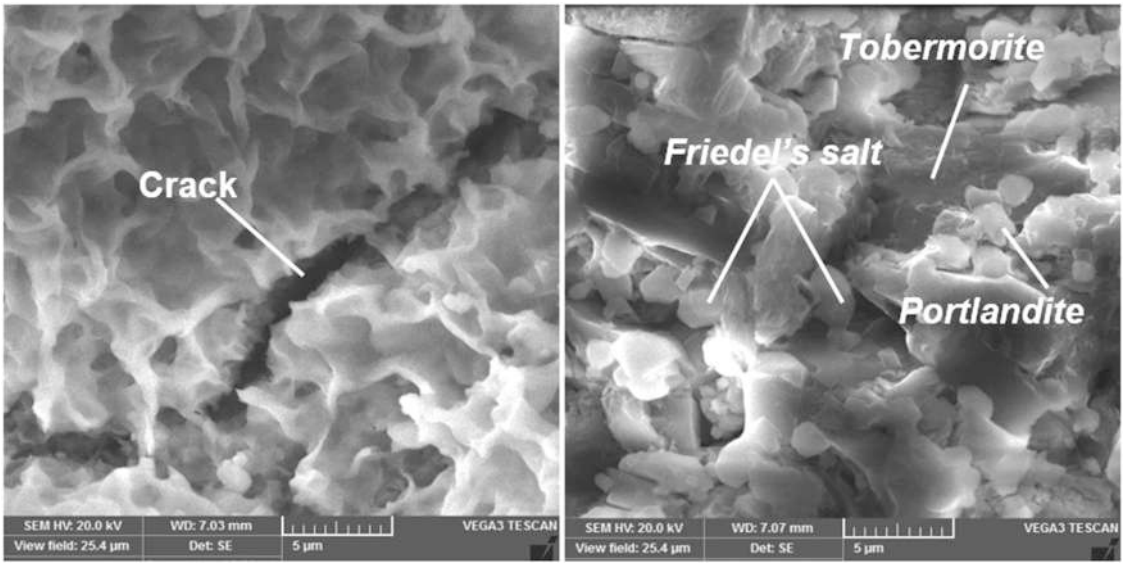

Fig. 8. Image of SEM microstructure of HPC-4 at 90 days.

Table 3
Results of petrography testing on the HPC cured in fresh water at 3 days, 7 days, 28 days, and 90 days.

Type of HPC	Age (day)	Pore (%)			Internal pore (*Intr-p*) (µm)		Isolated pore (*Isl-p*) (µm)	
		Concrete matrix	Aggregate	Amount	Minimum	Maximum	Minimum	Maximum
HPC-1	3	14.4	2	16.14	172.7	1106.8	9.2	20.4
	7	12	1.6	13.54	117.4	346.9	8.3	19.3
	28	10.71	1.85	12.38	110.5	249.9	3.3	17
	90	10.65	1.74	12.36	89.5	237.7	3.1	13.7

shows results of petrography testing on the HPC-1 cured in fresh water at 3days, 7 days, 28 days, and 90 days.

In hardened HPC, a pore is an empty volume in the cement matrix that contains only air. The type, size, shape, arrangement, and abundance of the pores are factors controlling chemical attack on the cement matrix. The percentage of air-pore volume is regularly specified by the design of the mixture of HPC [53]. A large quantity of very small air pores are suitable because it tends to shorten the average distance between any point in the paste and a pore, which was known a spacing factor. Therefore, the cement matrix is preserved from chemical attack e.g., chloride content and Friedel's salt. Besides, because pore is to weaken the HCC, spacing factor, which is much less than the maximum ensuring preservation from chemical attack, is inefficient and should be eluded [53]. From 3days to 90days, porosity of HPC-1 reduced 26%. Similar reducing trend is observed in internal pore and isolated pore in microstructure of HPC-1 (Table 3). Fig. 8 shows images of petrographic analyzis of HPC-1 cured in fresh water at 3 days, 7 days, 28 day, and 90 days. This figure also shows interaction among cement matrix and aggregate stack, porosity structure of HPC-1, intergranular pores, and isolated pores in the HPC-1.

Considering a non-pore microstructure in the HPC, it is well known that the interfacial transitition zone is feeble than concrete matrix, and hence fracturing in microstructure of concrete is commonly appeared in the ITZ. Then, micro-crack propagates in cement matrix and additional crack happens within mortar [54]. Regularly, gravel stack reacts elastically throughout the fracture process of concrete. Therefore, the isolated pore and intergranuler pore are an indicator for the continuum damaged plasticity (CDP) model [55, 56] used to construe the mechanic behavior of both cement-based solid materials. Percent of porosity, internal pore and isolated pore were established from petrographic investigation of the delicate piece of the HPC-1. Micro-cracks were also observed in the intersection between cement paste and aggregate stack in the HPCs. Microscopic examination of the coarse aggregate stack showed intergranular fractures (Fig. 9a, b, c, d). This data implies that during concrete curing, defects and fissures were enlarged in the highly serpentinized aggregate particle stack. Therefore, there is triggering defects and weaknesses in the HPC-1. Table 4 shows results of petrography testing on the HPC-2 cured in fresh water at 3 days, 7 days, 28 days, and 90 days.

From 3 days to 90 days, porosity of HPC-2 reduced 26.2%. Similar reducing trend is observed in internal pore and isolated pore in microstructure of HPC-2 (Table 4). HPC-2 showed a fine cohesion among cement matrix and aggregate stack. This could be attributed

both the binding capacity of chloride content, which was mentioned in introduction section, and the petrographic features of serpentine in the HPC-2. Fig. 10 shows images of petrographic analyzis of HPC-2 cured in fresh water at 3 days, 7 days, 28 day, and 90 days. This figure also shows interaction among cement matrix and aggregate stack, porosity structure of HPC-2, intergranular pores, and isolated pores in the HPC-2. Besides, in the total of HPC-2 cured in sea water led to chloride content and Friedel's salt as of 3days, a reaction zone of chemical attack was detected a few microns thick (Fig. 10).

Unlike HPC-1, the sea water curing provided a better cohesion for the cement matrix of HPC-2. Nevertheless, there was shown vein as well as internal pore and isolated pore in the cement paste of HPC-2 (Fig. 10a, b, c, d). HPC-2 manufactured with water of fresh and cured in water of sea, on the other hand, had greater cohesiveness than HPC-1 made with fresh water and cured in fresh water, HPC-3 made with water of sea and cured in water of sea, and HPC-4 made with water of sea and cured in air. In regularly, the water of sea curing presented the greatest cohesion in the work. Zone of local reaction was also discovered surrounding and inside the aggregate particle stack's micro-cracks (Fig. 10a, b, c, d). The thin section's comprehensive analysis showed concentrate on the aggregate stack-to-cement matrix fragment contact angel and identify several distinguishing characteristics [57]. In reality, numerous sorts of contact angles exist depending on whether the aggregate's surface is smooth or contains defects caused by the fragment. Fig. 10 shows not only interpenetration between the two parts, aggregate and cement matrix, but also direct touching with a consistent and regular pattern. Usually, the paste of cement seems to have had a significant interaction with the aggregate stack, since the chloride binding aids the development of a complete link between the two components. Besides, it must be noted that such fragment being analyzed obtained from the HPC-2, and therefore such connection may be due to binding of chloride and salt of Friedel. Despite this, it is achievable to

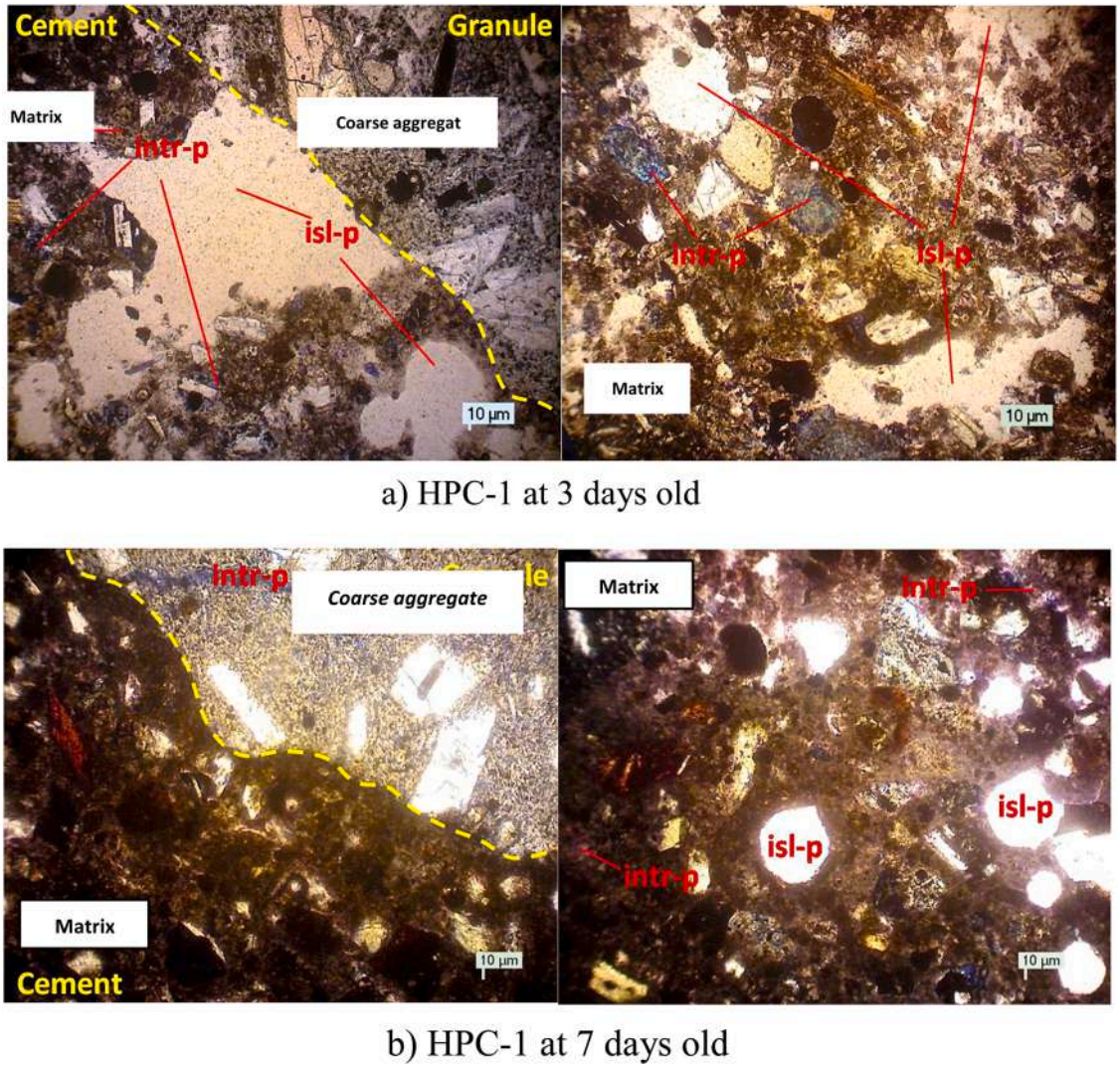

Fig. 9. Images of petrographic analyzis of HPC-1 cured in fresh water at 3 days, 7 days, 28 day, and 90 days- interaction among cement matrix and aggregate stack, porosity structure of HPC-1, intergranular pores, and isolated pores in the HPC-1.

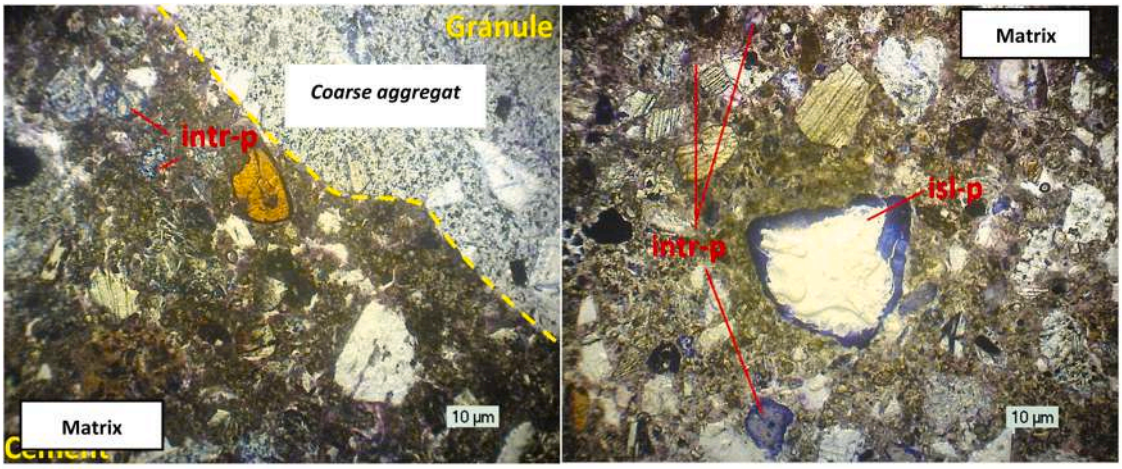

c) HPC-1 at 28 days old

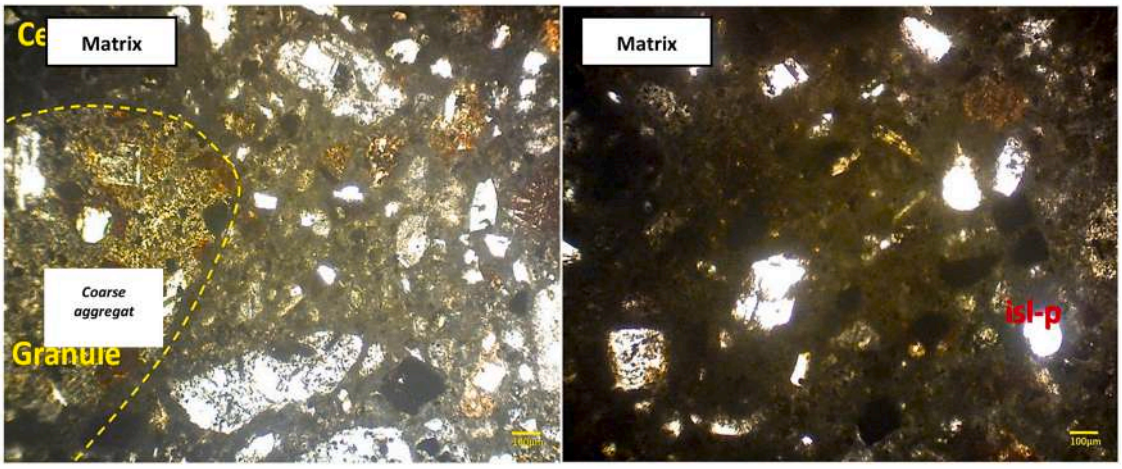

d) HSC-1 at 90 days old

Fig. 9. (*continued*).

note that the angel between cement matrix and aggregate stack is roughly, continuous, and regular (Fig. 10a, b, c, d). This apparent interaction among the two components could be seen above all on the fragment at 3 days, 7 days, 28 days, and 90 days. This indicates that the cement paste has taken up the usual course of the gravel stack. Therefore, the adhesion is a sign that is clearly better than that of HPC-1, HPC-3, and HPC-4. Table 5 shows results of petrography testing on the HPC-3 cured in fresh water at 3 days, 7 days, 28 days, and 90 days.

Because HPC-3 was combined with water of sea and cured in water of sea, its porosity decreased by 19% from 3 day to 90 days. Similar reducing trend was observed in internal pore and isolated pore in microstructure of HPC-3 (Table 5). Such kind of evaluation was also made by Winslow and Liu previously. They discovered that the porosity of concrete paste is high, and that the difference in

Table 4
Results of petrography testing on the HPC-2 in seawater.

Type of HPC	Curing age (Day)	Pore (%)			Internal pore (µm)		Isolated pore (µm)	
		Concrete matrix	Aggregate	Amount	Minimum	Maximum	Minimum	Maximum
HPC-2	3	14.4	2	16.14	172.7	1106.8	9.2	20.4
	7	11.8	2.05	13.54	117.4	346.9	8.3	19.3
	28	10.64	2.2	12.38	110.5	249.9	3.3	17
	90	10.62	2.05	12.36	89.5	237.7	3.1	13.7

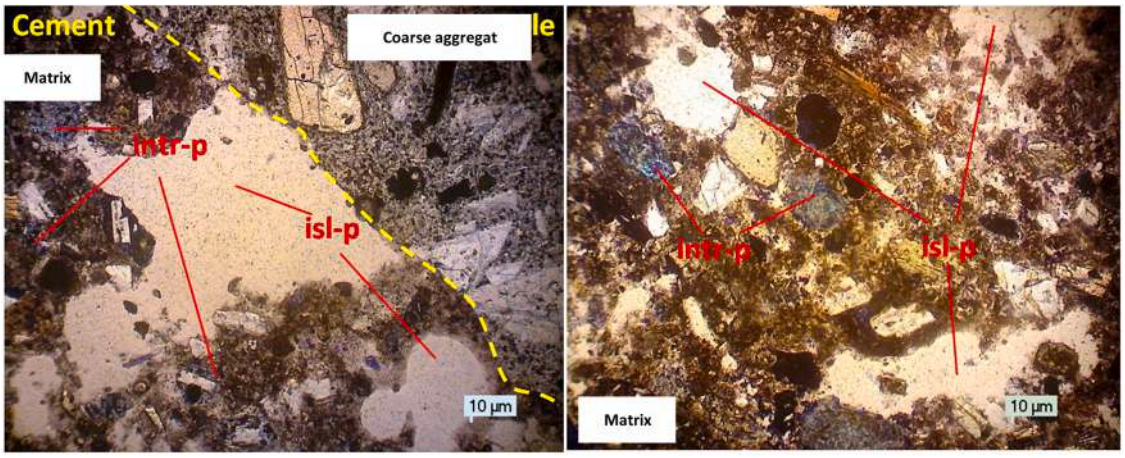

a) HPC-2 at 3 days old

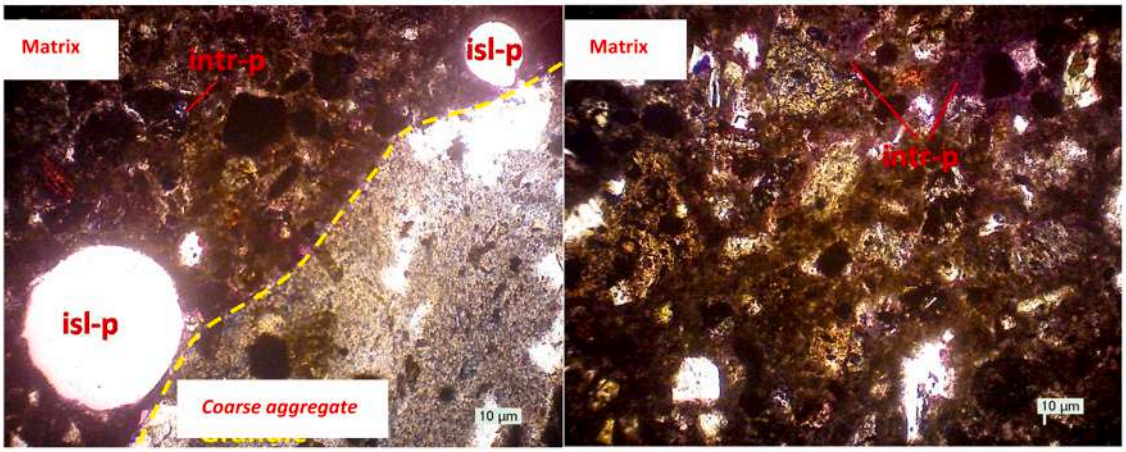

b) HPC-2 at 7 days old

Fig. 10. Images of petrographic analyzis of HPC-2 cured in fresh water at 3 days, 7days, 28 day, and 90 days- interaction among cement matrix and aggregate stack, porosity structure of HPC-2, intergranular pores, and isolated pores in the HPC-2.

porosity grows as hydration increases. Additional a bigger porosity is mostly found in the ordinary paste's entrance pore width, such as internal pore and isolated pore [58]. Fig. 11 shows images of petrographic analyzis of HPC-3 cured in sea water at 3 days, 7 days, 28 day, and 90 days. This figure also shows interaction among cement matrix and aggregate stack, porosity structure of HPC-3, intergranular pores, and isolated pores in the HPC-3.

In addition to the fact that mentioned above, like HPC-2, the water of sea curing provided a better cohesion for the cement matrix of HPC-3. Despite there was shown unvein structure, it was clearly observed the internal pore and isolated pore in the cement paste of HPC-3 (Fig. 11a, b, c, d). HPC-3 manufactured with sea water and cured in sea water, on the other hand, had greater cohesiveness than HPC-1 made with water of fresh and cured in water of fresh, HPC-2 made with water of fresh and cured in water of sea, and HPC-4 made with sea water and cured in air. In the study, the curing water of sea of HPC-3 combined with water of sea produced lower cohesiveness than the curing water of sea of HPC-2. Zone of local reaction was also discovered surrounding and inside the aggregate particle stack's micro-cracks (Fig. 11a, b, c, d). Table 6 shows results of petrography testing on the HPC-4 cured in fresh water at 3 days, 7 days, 28 days, and 90 days.

From 3 days to 90 days, porosity of HPC-4 reduced only 8.3%, because the HPC-4 was mixed with water of sea and cured in air. In other words, it was not treated like HPC-3 which was mixed with water of sea and cured in water of sea. This kind treatment results in increase in cohesion and reducing in internal pore and isolated pore. Similar reducing trend was observed in internal pore and isolated pore in microstructure of HPC-3 (Table 6). Porosity of HPC-4 is bigger than that of both HPC-1, HPC-2, and HPC-3 at 90 days. This could be attributed that air curing for HPC mixed with sea water is not useful and, though HPCs have same ingredients, the air curing

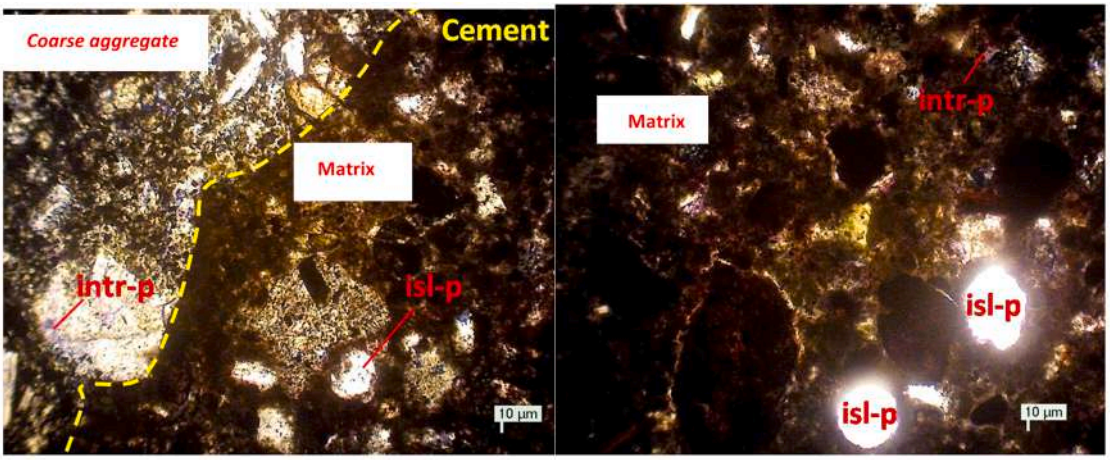

c) HPC-2 at 28 days old

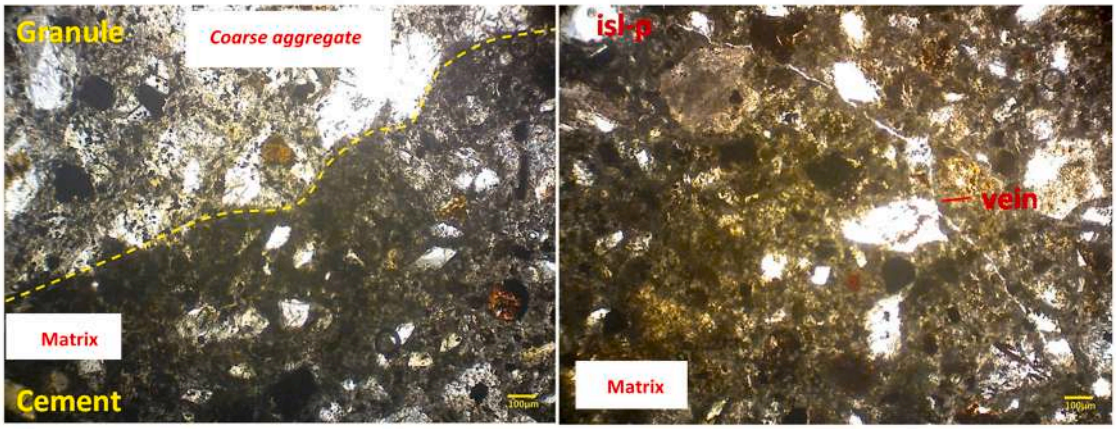

d) HPC-2 at 90 days old

Fig. 10. (*continued*).

Table 5
Results of petrography testing on the HPC-3 in fresh water at 3 days, 7 days, 28 days, and 90 days.

Type of HPC	Curing age (Day)	Pore (%)			Internal pore (μm)		Isolated pore (μm)	
		Concrete matrix	Aggregate	Amount	Minimum	Maximum	Minimum	Maximum
HPC-3	3	13.05	1.65	14.79	119.8	666.6	6.4	18.6
	7	11.2	1.2	12.94	90.2	332.4	5	19.5
	28	10.62	1.64	12.36	79.5	233.4	3.9	15.1
	90	10.50	1.50	12.24	50.5	233.1	1.9	12

retards the binding capacity of chloride in the HPC-4. As the water/cement was kept constant, the porosity of HPC-4 was not increase with hydration, like being in the work which was conducted by Winslow and Liu [58]. Fig. 12 shows images of petrographic analyzis of HPC-4 cured in air at 3 days, 7 days, 28 days, and 90 days. This figure also shows interaction among cement matrix and aggregate stack, porosity structure of HPC-4, intergranular pores, and isolated pores in the HPC-4.

Additionally, other critical factor is the need for the usage of superplasticizer in HPC with the same slump. This reduction in water is required because to the HPC's decreased porosity, that makes the concrete much adhesive. As a result, it is concluded that superplasticizer and sea water curing indicate increased resistance to chemical assault by chloride and salt of Friedel. It could not be an issue since the cement content would not have to be increased to maintain the requisite w/c ratio, which would result in a reduction in the ultimate cost of the HPC mixture [59]. It should also be noted that the HPC that is workable easily is desirable material guaranteed by the right water/cement. In terms of porosity, the HPC-4 has greater internal pore and isolated pore than that of both HPC-1, HPC-2, and

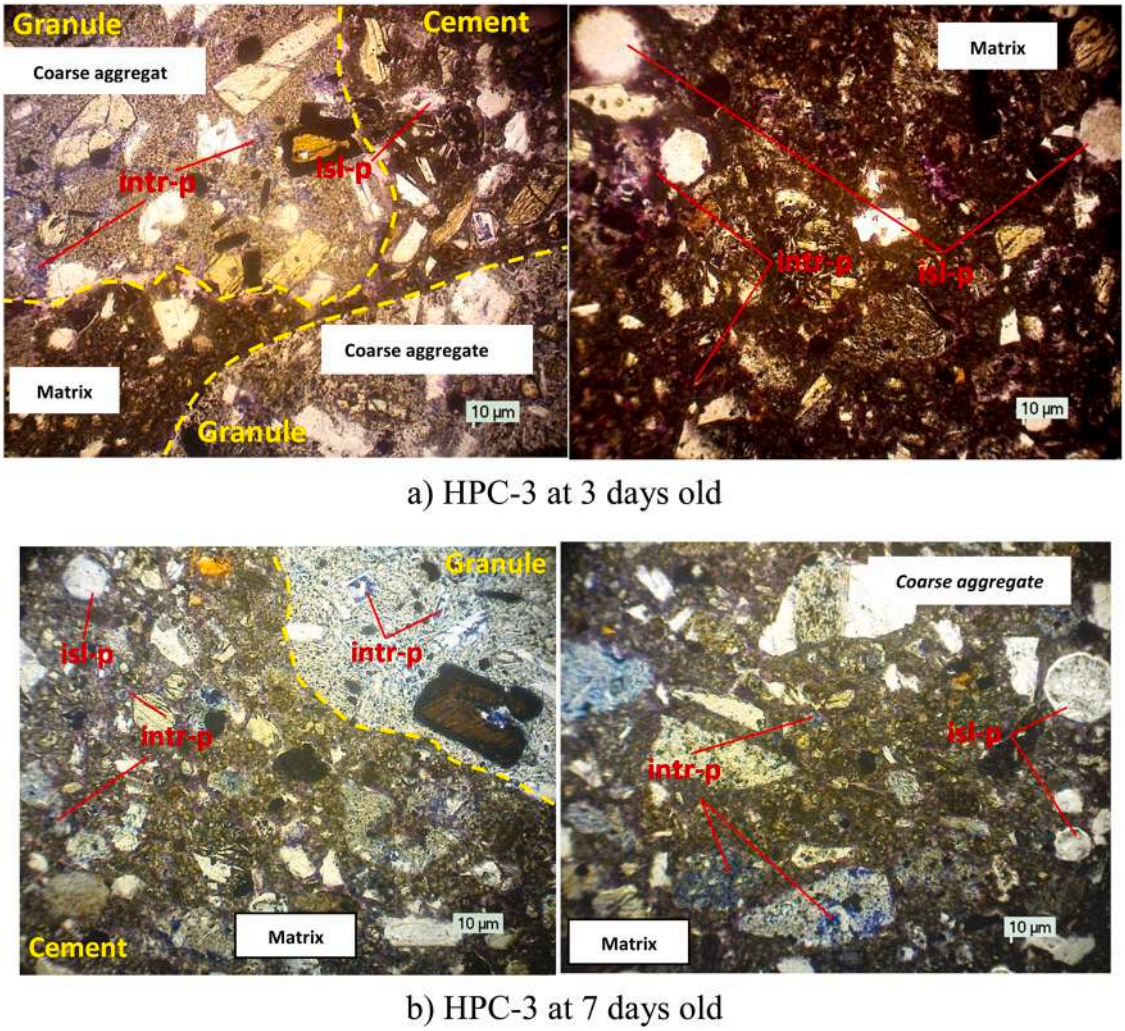

Fig. 11. Images of petrographic analyzis of HPC-3 cured in sea water at 3days, 7days, 28 day, and 90days- interaction among cement matrix and aggregate stack, porosity structure of HPC-3, intergranular pores, and isolated pores in the HPC-3.

HPC3, because it encountered a combined influence, e.g., mixing of sea water and curing in air (Fig. 12). The combined influence results in improper hydration and poros media in microstructure of HPC. This could be attributed that the mechanism of air curing opens disconnections among cement matrix and aggregate stack in the HPC-4.

4. Conclusions

The entry of chloride and the formation of Friedel's salt in HPC is the effect of the water used as mixing and treatment water. HPC-1 found no chloride and Friedel's salt. In HPC-2, no chloride and Friedel salt were found after 3 days of treatment with seawater, but after 7 days, the chloride had entered and Friedel's salt was formed in HPC. Because HPC uses seawater as a mixing water, HPC-1 and HPC-3 discovered chloride and friedel salt. The amount of chloride and friedel salt increased with increasing curing time.

The amount of portlandite, tobermorite, and etringite compounds in all types of HPC increased with the curing time or the age of the concrete. On the other hand, the amount of tricalcium silicate and dicalcium silicate decreases with increasing curing time or the age of the concrete. The number of HPC tobermorite using seawater as mixing and curing water was greater than HPC using fresh water at an early age (3 days), but the porosity value was lower.

The concrete mixed with seawater and treated with seawater increases the hydration components of tobermorite and ettringite as well as concrete in general. The SEM analysis supports the data obtained in the XRD analysis. Similar increases and decelerations in the

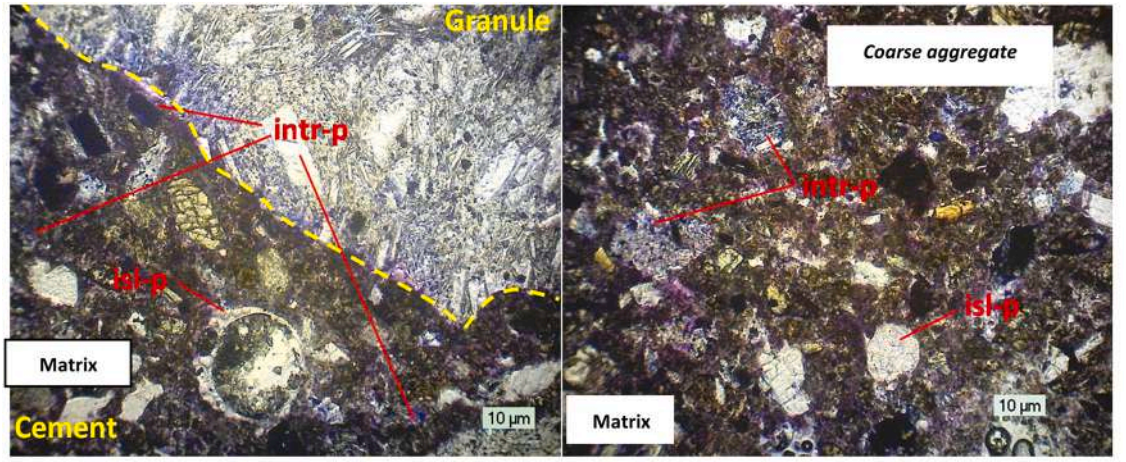

c) HPC-3 at 28 days old

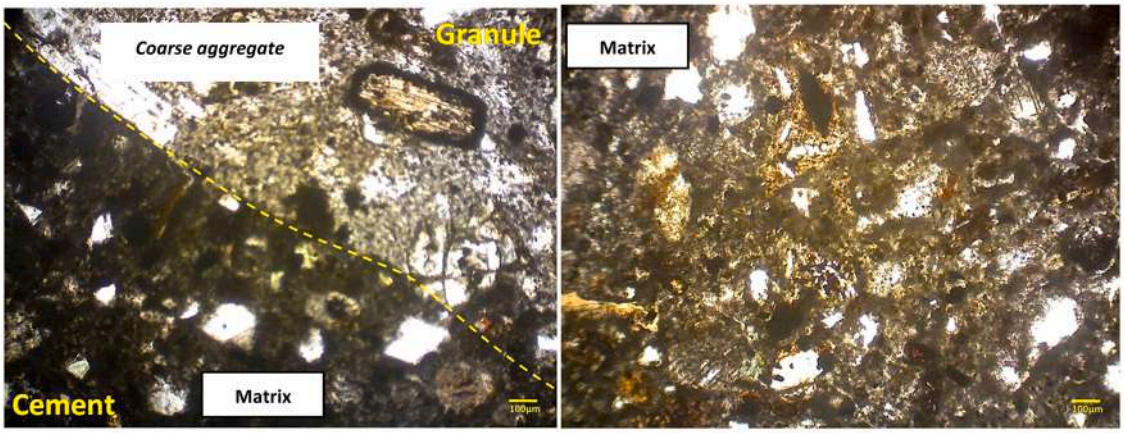

d) HPC-3 at 90 days old

Fig. 11. (*continued*).

Table 6
Results of petrography testing on the HPC-4 cured in fresh water at 3 days, 7 days, 28 days, and 90 days.

Type of HPC	Curing age (day)	Pore (%)			Internal pore (µm)		Isolated pore (µm)	
		Concrete matrix	Aggregate	Amount	Minimum	Maximum	Minimum	Maximum
HPC-4	3	13.05	1.65	14.79	119.8	666.6	6.4	18.6
	7	12.6	1.2	14.34	114.5	560.4	9	19.1
	28	12	2	13.74	108.1	490.2	8	18.8
	90	11.96	1.44	13.70	106.3	416.7	5.2	19.8

hydration component were shown in the SEM analysis of the HPC. Petrographic analysis and porosity testing are provided to understand the micropore structure, for example, internal pores and isolated pores in HPC and reduced porosity in HPC mixed with seawater and cured in seawater. In this study, HPC-3 showed the highest performance in terms of component hydration, SEM observations, porosity, and petrographic analysis.

Declaration of Competing Interest

The authors declare that they have no known competing financial interests or personal relationships that could have appeared to influence the work reported in this paper.

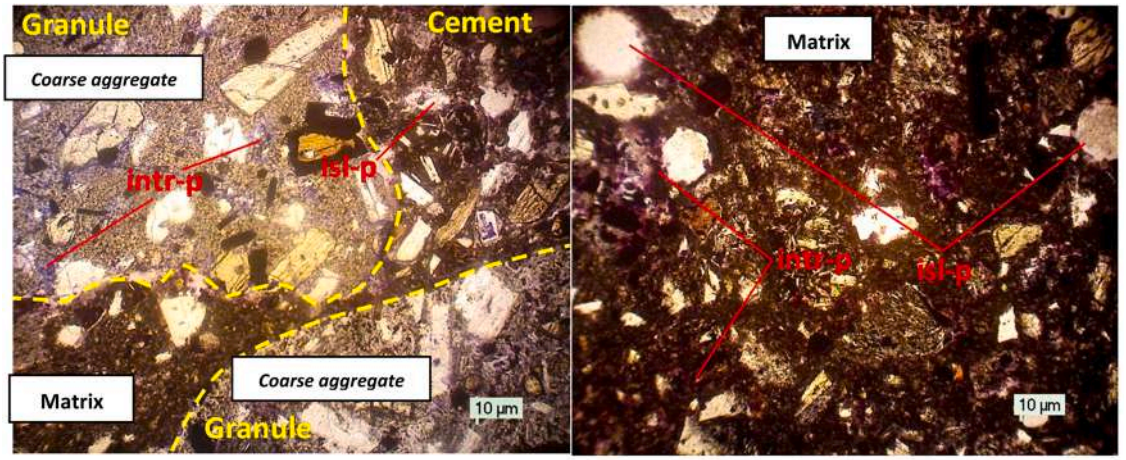

a) HPC-4 at 3 days old

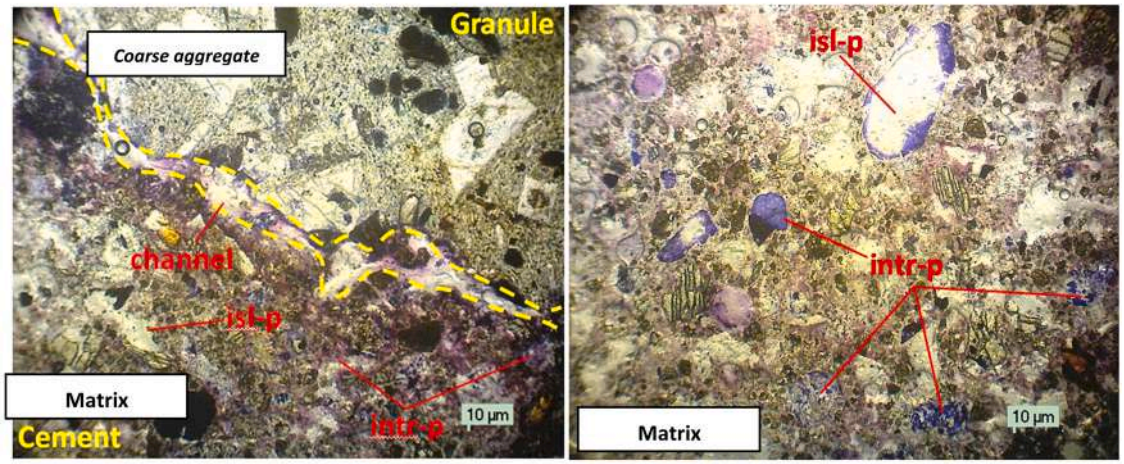

b) HPC-4 at 7 days old

Fig. 12. Images of petrographic analyzis of HPC-4 cured in air at 3 days, 7 days, 28 day, and 90 days- interaction among cement matrix and aggregate stack, porosity structure of HPC-4, intergranular pores, and isolated pores in the HPC-4.

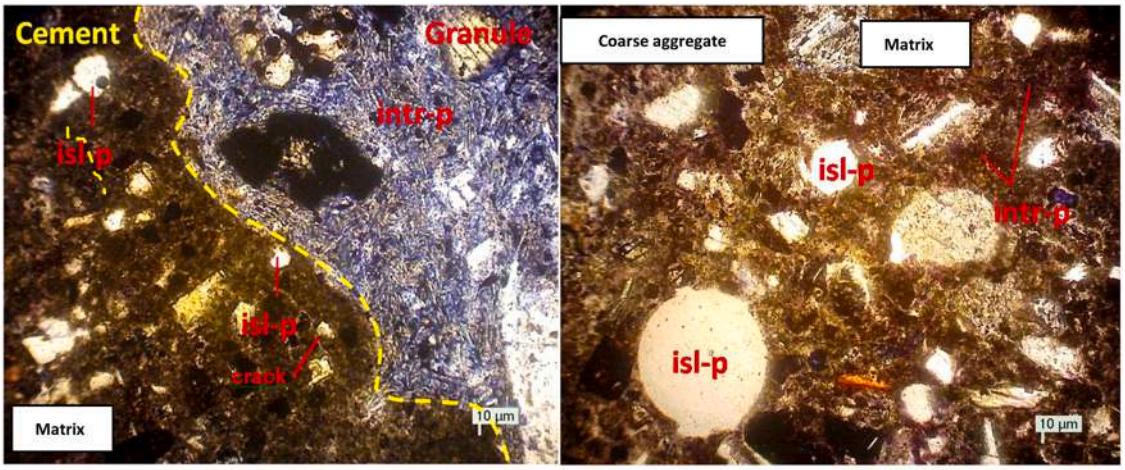

c) HPC-4 at 28 days old

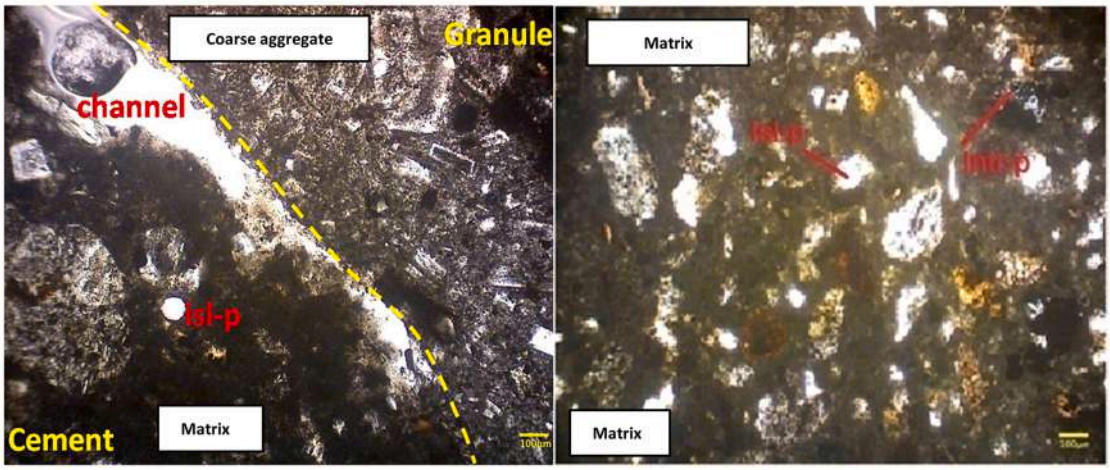

d) HPC-4 at 90 days old

Fig. 12. (*continued*).

References

[1] F. Qu, W. Li, W. Dong, V.W.Y. Tam, T. Yu, Durability deterioration of concrete under marine environment from material to structure: a critical review, J. Build. Eng. 35 (2021), 102074, https://doi.org/10.1016/J.JOBE.2020.102074.
[2] H.Y. Wang, A study of the effects of LCD glass sand on the properties of concrete, Waste Manag. 29 (2009) 335–341, https://doi.org/10.1016/J.WASMAN.2008.03.005.
[3] W. Shao, D. Shi, Probabilistic analysis of the durability of piles with microcracks under chloride attack, Int. J. Concr. Struct. Mater. 15 (2021) 1–12, https://doi.org/10.1186/S40069-021-00478-5/FIGURES/11.
[4] A. Ahmed, S. Guo, Z. Zhang, C. Shi, D. Zhu, A review on durability of fiber reinforced polymer (FRP) bars reinforced seawater sea sand concrete, Constr. Build. Mater. 256 (2020), 119484, https://doi.org/10.1016/J.CONBUILDMAT.2020.119484.
[5] Y.L. Li, J.G. Teng, X.L. Zhao, R.K. Singh Raman, Theoretical model for seawater and sea sand concrete-filled circular FRP tubular stub columns under axial compression, Eng. Struct. 160 (2018) 71–84, https://doi.org/10.1016/J.ENGSTRUCT.2018.01.017.
[6] A. Zhou, C.L. Chow, D. Lau, Structural behavior of GFRP reinforced concrete columns under the influence of chloride at casting and service stages, Compos. Part B: Eng. 136 (2018) 1–9, https://doi.org/10.1016/J.COMPOSITESB.2017.10.011.
[7] A.R. Murthy, N.R. Iyer, B.K.R. Prasad, Evaluation of mechanical properties for high strength and ultrahigh strength concretes, Adv. Concr. Constr. 1 (2013) 341–358, https://doi.org/10.12989/ACC2013.1.4.341.
[8] S.A. Ghahari, A.M. Ramezanianpour, A.A. Ramezanianpour, M. Esmaeili, An accelerated test method of simultaneous carbonation and chloride ion ingress: durability of silica fume concrete in severe environments, 2016, Vol. 2016, Pages 1-12, Adv. Mater. Sci. Eng. 2016 (2016) 1–12, https://doi.org/10.1155/2016/1650979.
[9] W. Qiang Jiang, X. Han Shen, J. Xia, L. Xuan Mao, J. Yang, Q. Feng Liu, A numerical study on chloride diffusion in freeze-thaw affected concrete, Constr. Build. Mater. 179 (2018) 553–565, https://doi.org/10.1016/J.CONBUILDMAT.2018.05.209.
[10] J. Liu, G. Ou, Q. Qiu, X. Chen, J. Hong, F. Xing, Chloride transport and microstructure of concrete with/without fly ash under atmospheric chloride condition, Constr. Build. Mater. 146 (2017) 493–501, https://doi.org/10.1016/J.CONBUILDMAT.2017.04.018.
[11] X. Zhu, G. Zi, W. Lee, S. Kim, J. Kong, Probabilistic analysis of reinforcement corrosion due to the combined action of carbonation and chloride ingress in concrete, Constr. Build. Mater. 124 (2016) 667–680, https://doi.org/10.1016/J.CONBUILDMAT.2016.07.120.

[12] Q. Feng Liu, G. Lin Feng, J. Xia, J. Yang, L. Yuan Li, Ionic transport features in concrete composites containing various shaped aggregates: a numerical study, Compos. Struct. 183 (2018) 371–380, https://doi.org/10.1016/J.COMPSTRUCT.2017.03.088.
[13] A. Ipavec, T. Vuk, R. Gabrovšek, V. Kaučič, Chloride binding into hydrated blended cements: the influence of limestone and alkalinity, Cem. Concr. Res. 48 (2013) 74–85, https://doi.org/10.1016/J.CEMCONRES.2013.02.010.
[14] Y. Zhou, D. Hou, J. Jiang, L. Liu, W. She, J. Yu, Experimental and molecular dynamics studies on the transport and adsorption of chloride ions in the nano-pores of calcium silicate phase: the influence of calcium to silicate ratios, Microporous Mesoporous Mater. 255 (2018) 23–35, https://doi.org/10.1016/J.MICROMESO.2017.07.024.
[15] Q. Yuan, C. Shi, G. de Schutter, K. Audenaert, D. Deng, Chloride binding of cement-based materials subjected to external chloride environment – A review, Constr. Build. Mater. 23 (2009) 1–13, https://doi.org/10.1016/J.CONBUILDMAT.2008.02.004.
[16] W. Qiang Jiang, X. Han Shen, S. Hong, Z. Yan Wu, Q. Feng Liu, Binding capacity and diffusivity of concrete subjected to freeze-thaw and chloride attack: A numerical study, Ocean Eng. 186 (2019), 106093, https://doi.org/10.1016/J.OCEANENG.2019.05.075.
[17] M.M. Wang, B.M. Fan, B.Y. Wen, C. Jiang, Experimental and theoretical studies on the removal mechanism of formaldehyde from water by mesoporous calcium silicate, 2020 63:10, Sci. China Technol. Sci. 63 (2020) 2098–2112, https://doi.org/10.1007/S11431-019-1504-7.
[18] Q. Yuan, C. Shi, G. de Schutter, K. Audenaert, D. Deng, Chloride binding of cement-based materials subjected to external chloride environment – A review, Constr. Build. Mater. 23 (2009) 1–13, https://doi.org/10.1016/J.CONBUILDMAT.2008.02.004.
[19] A. Khitab, S. Lorente, J.P. Ollivier, Predictive model for chloride penetration through concrete, Http://Dx.Doi.Org/10.1680/Macr.2005.57.9.511 57 (2015) 511–520, https://doi.org/10.1680/MACR.2005.57.9.511.
[20] M.V.A. Florea, H.J.H. Brouwers, Chloride binding related to hydration products: Part I: Ordinary Portland cement, Cem. Concr. Res. 42 (2012) 282–290, https://doi.org/10.1016/J.CEMCONRES.2011.09.016.
[21] H. Chang, Chloride binding capacity of pastes influenced by carbonation under three conditions, Cem. Concr. Compos. 84 (2017) 1–9, https://doi.org/10.1016/J.CEMCONCOMP.2017.08.011.
[22] P. Wang, Y. Jia, T. Li, D. Hou, Q. Zheng, Molecular dynamics study on ions and water confined in the nanometer channel of Friedel's salt: structure, dynamics and interfacial interaction, Phys. Chem. Chem. Phys. 20 (2018) 27049–27058, https://doi.org/10.1039/C8CP02450B.
[23] M. Salhi, M. Ghrici, A. Li, T. Bilir, Effect of curing treatments on the material properties of hardened self-compacting concrete, Adv. Concr. Constr. 5 (2017) 359–375, https://doi.org/10.12989/ACC.2017.5.4.359.
[24] A.A. Patil, H.S. Chore, P.A. Dodeb, Effect of curing condition on strength of geopolymer concrete, Adv. Concr. Constr. 2 (2014) 29–37, https://doi.org/10.12989/ACC.2014.2.1.029.
[25] A.K. Parande, Role of ingredients for high strength and high performance concrete - A review, Adv. Concr. Constr. 1 (2013) 151–162, https://doi.org/10.12989/ACC.2013.01.2.151.
[26] O.A. Qasim, B.H. Maula, H.H. Moula, S.H. Jassam, Effect of salinity on concrete properties, IOP Conf. Ser.: Mater. Sci. Eng. 745 (2020), https://doi.org/10.1088/1757-899X/745/1/012171.
[27] J.-G. Teng, Y. Xiang, T. Yu, Z. Fang, Development and mechanical behaviour of ultra-high-performance seawater sea-sand concrete, Adv. Struct. Eng. 22 (2019) 3100–3120, https://doi.org/10.1177/1369433219858291.
[28] B. Erniati, The self compacting concrete (SCC) using seawater as mixing water without curing, ARPN J. Eng. Appl. Sci. 13 (2018) 4057–4061, https://doi.org/10.31227/osf.io/pujv7.
[29] Erniati, M.W. Tjaronge, R. Djamaluddin, V. Sampebulu, Porosity and microstructure phase of self compacting concrete using sea water as mixing water and curing, Adv. Mater. Res. 1119 (2015) 647–651, https://doi.org/10.4028/www.scientific.net/amr.1119.647.
[30] Erniati, M.W. Tjaronge, R. Djamaluddin, V. Sampebulu, Compressive strength and slump flow of self compacting concrete uses fresh water and sea water, ARPN J. Eng. Appl. Sci. 10 (2015) 2373–2377.
[31] R. Irmawaty, M.W. Tjaronge, Effect of Seawater as Mixing Water on the Mechanical Properties of Mortar and Concrete, in: ConCERN (Conference for Civil Engineering Research Networks) 2014, 2014: pp. 61–64.
[32] J.-G. Teng, Y. Xiang, T. Yu, Z. Fang, Development and mechanical behaviour of ultra-high-performance seawater sea-sand concrete, Adv. Struct. Eng. 22 (14) (2019) 3100–3120, https://doi.org/10.1177/1369433219858291.
[33] EFNARC, The European Guidelines for Self-Compacting Concrete: Specification, Production and Use, UK, 2005.
[34] ASTM C1365–18, Standard Test Method for Determination of the Proportion of Phases in Portland Cement and Portland-Cement Clinker Using X-Ray Powder Diffraction Analysis, West Conshohocken, PA, 2018.
[35] ASTM C642 - 13, Standard Test Method for Density, Absorption, and Voids in Hardened Concrete, West Conshohocken, PA, 2013.
[36] ASTM C856/C856M-20, Standard Practice for Petrographic Examination of Hardened Concrete, West Conshohocken, PA, 2020.
[37] W.P.S. Dias, Reduction of concrete sorptivity with age through carbonation, Cem. Concr. Res. 30 (2000) 1255–1261, https://doi.org/10.1016/S0008-8846(00)00311-2.
[38] V.G. Papadakis, M.N. Fardis, C.G. Vayenas, Effect of composition, environmental factors and cement-lime mortar coating on concrete carbonation, 1992 25:5, Mater. Struct. 25 (1992) 293–304, https://doi.org/10.1007/BF02472670.
[39] P. Li, W. Li, T. Yu, F. Qu, V.W.Y. Tam, Investigation on early-age hydration, mechanical properties and microstructure of seawater sea sand cement mortar, Constr. Build. Mater. 249 (2020), 118776, https://doi.org/10.1016/J.CONBUILDMAT.2020.118776.
[40] A. Younis, U. Ebead, P. Suraneni, A. Nanni, Fresh and hardened properties of seawater-mixed concrete, Constr. Build. Mater. 190 (2018) 276–286, https://doi.org/10.1016/J.CONBUILDMAT.2018.09.126.
[41] S. Han, J. Zhong, W. Ding, J. Ou, Strength, hydration, and microstructure of seawater sea-sand concrete using high-ferrite Portland cement, Constr. Build. Mater. 295 (2021), 123703, https://doi.org/10.1016/J.CONBUILDMAT.2021.123703.
[42] X.F. Wang, Z.J. Yang, J.R. Yates, A.P. Jivkov, C. Zhang, Monte Carlo simulations of mesoscale fracture modelling of concrete with random aggregates and pores, Constr. Build. Mater. 75 (2015) 35–45, https://doi.org/10.1016/J.CONBUILDMAT.2014.09.069.
[43] X. Wang, M. Zhang, A.P. Jivkov, Computational technology for analysis of 3D meso-structure effects on damage and failure of concrete, Int. J. Solids Struct. 80 (2016) 310–333, https://doi.org/10.1016/J.IJSOLSTR.2015.11.018.
[44] S. Diamond, A critical comparison of mercury porosimetry and capillary condensation pore size distributions of portland cement pastes, Cem. Concr. Res. 1 (1971) 531–545, https://doi.org/10.1016/0008-8846(71)90058-5.
[45] R. Kumar, B. Bhattacharjee, Porosity, pore size distribution and in situ strength of concrete, Cem. Concr. Res. 33 (2003) 155–164, https://doi.org/10.1016/S0008-8846(02)00942-0.
[46] M. Rößler, I. Odler, Investigations on the relationship between porosity, structure and strength of hydrated portland cement pastes I. Effect of porosity, Cem. Concr. Res. 15 (1985) 320–330, https://doi.org/10.1016/0008-8846(85)90044-4.
[47] X. Chen, S. Wu, J. Zhou, Influence of porosity on compressive and tensile strength of cement mortar, Constr. Build. Mater. 40 (2013) 869–874, https://doi.org/10.1016/J.CONBUILDMAT.2012.11.072.
[48] D.P.H. Hasselman, Griffith flaws and the effect of porosity on tensile strength of brittle ceramics, 457–457, J. Am. Ceram. Soc. 52 (1969), https://doi.org/10.1111/J.1151-2916.1969.TB11982.X.
[49] K.K. Schiller, Strength of porous materials, Cem. Concr. Res. 1 (1971) 419–422, https://doi.org/10.1016/0008-8846(71)90035-4.
[50] E. Ryshkewitch, Compression strength of porous sintered alumina and zirconia, J. Am. Ceram. Soc. 36 (1953) 65–68, https://doi.org/10.1111/J.1151-2916.1953.TB12837.X.
[51] S. Mindess, Concrete, Prentice Hall,, 2002, p. 644.
[52] C.C. Yang, S.W. Cho, L.C. Wang, The relationship between pore structure and chloride diffusivity from ponding test in cement-based materials, Mater. Chem. Phys. 100 (2006) 203–210, https://doi.org/10.1016/J.MATCHEMPHYS.2005.12.032.

[53] M.J. McCarthy, T.D. Dyer, Pozzolanas and pozzolanic materials, Lea's Chem. Cem. Concr. (2019) 363–467, https://doi.org/10.1016/B978-0-08-100773-0.00009-5.
[54] J.F. Unger, S. Eckardt, Multiscale modeling of concrete, 2011 18:3, Arch. Comput. Methods Eng. 18 (2011) 341–393, https://doi.org/10.1007/S11831-011-9063-8.
[55] J. Lee, G.L. Fenves, Plastic-damage model for cyclic loading of concrete structures, J. Eng. Mech. 124 (1998) 892–900, https://doi.org/10.1061/(ASCE)0733-9399(1998)124:8(892).
[56] J. Lubliner, J. Oliver, S. Oller, E. Oñate, A plastic-damage model for concrete, Int. J. Solids Struct. 25 (1989) 299–326, https://doi.org/10.1016/0020-7683(89)90050-4.
[57] G. Lacidogna, G. Piana, F. Accornero, A. Carpinteri, Multi-technique damage monitoring of concrete beams: acoustic emission, digital image correlation, dynamic identification, Constr. Build. Mater. 242 (2020), 118114, https://doi.org/10.1016/J.CONBUILDMAT.2020.118114.
[58] D. Winslow, D. Liu, The pore structure of paste in concrete, Cem. Concr. Res. 20 (1990) 227–235, https://doi.org/10.1016/0008-8846(90)90075-9.
[59] T. Santana, J. Gonçalves, F. Pinho, R. Micaelo, Effects of the ratio of porosity to volumetric cement content on the unconfined compressive strength of cement bound fine grained soils, 2021, Vol. 6, Page 96, Infrastructures 6 (2021) 96, https://doi.org/10.3390/INFRASTRUCTURES6070096.